North Sea Flow Measurement Workshop
22 – 25th October 2013

FLOW MEASUREMENT OF HIGH VISCOSITY FLUIDS

Chris Mills, Craig Marshall, Andy Kay, Marc MacDonald NEL.

1 INTRODUCTION

The vast majority of the world's remaining oil reserves are categorised as heavy / unconventional oils (high viscosity). Due to diminishing conventional oil reserves and the need to secure future energy supplies to a rising world population, the exploitation of unconventional oils will increase. As the development of these viscous deposits grows, so too will the requirement for accurate flow measurement of heavy crude oils and other viscous products.

Unfortunately, the performance of conventional flowmeters when applied to viscous fluids[1] remains relatively poorly known. However, a number of technical challenges are immediately identifiable. These include the higher viscous friction of the fluid being metered, the possibility of extreme or varying velocity profiles, and the increased susceptibility of viscous liquids to entrain secondary components such as solids or gas. It is reasonable to predict that different metering devices will be affected by these phenomena in different ways, but to date the most appropriate technologies for viscous flow measurement are not yet well defined.

Well established flow measurement technologies such as differential pressure devices are known to be sensitive to viscosity variations. However there is little published data on their performance across a range of viscosities and Reynolds number. The same can also be said for "newer" measurement technologies such as Coriolis and ultrasonic devices. Confusion can arise when flowmeter manufacturer's make specific claims on performance with little independent and verifiable data published. This follows partly from the scarcity of suitable test facilities capable of providing viscous flow in combination with accurate and traceable reference instrumentation.

To improve this situation, NEL has completed an investigative programme into the performance of two Coriolis, three ultrasonic, two Venturi tubes and two quadrant edge orifice plates when evaluated across a range of high viscosity conditions. This paper reports on the response of these devices when operated from nominally 100 – 1500 cSt at the UK National Standards Oil Flow Facility at NEL in Glasgow, Scotland.

2 FLOW MEASUREMENT CHALLENGES

Flow measurement of 'medium' and 'heavy' crude oils present additional technical challenges compared to 'light' crude oils due to their greater viscous friction. Challenges such as irregular flow regimes and varying viscosity will be discussed in more detail in the sections below.

[1] For the purpose of this paper, 'high' viscosity in relation to hydrocarbon liquids, is taken as a kinematic viscosity > 100 cSt.

2.1 Characteristics of Viscous Fluids

2.1.1 Flow Regime

The level of force exerted due to viscous friction can be characterised by its viscosity coefficient. The absolute viscosity of a fluid can be expressed in centi-Poise (cP). The higher the value of absolute viscosity, the greater the frictional viscous forces on the pipe wall. As an example, the viscosities of some common fluids are listed in Table 1.

Table 1 – Fluid viscosity

Fluid Type	Viscosity at 20 °C (cP)
Water	1
Engine Oil	100
Gear Oil	1000
Honey	10000

Another often quoted definition for viscosity is the kinematic viscosity. It is defined as the ratio of the fluid's dynamic viscosity to its density and is generally quoted in centi-Stokes (cSt). The SI units are m^2/s and the unit conversion is 1 m^2/s = 1 x 10^6 cSt.

For most liquids, an increase in temperature normally results in a decrease in fluid viscosity. The decline in viscosity with increasing temperature is generally far greater for highly viscous fluids and can pose several problems. Figure 1 displays the kinematic viscosity of two NEL test fluids, one light and one heavy, plotted against fluid temperature.

Problems can arise in the flow measurement of viscous fluids when small fluctuations in temperature result in a significant change in the fluid viscosity. If the flowmeter has been calibrated at a specific viscosity for its application, any temperature and thus viscosity fluctuation could potentially have a notable effect on the flow measurement.

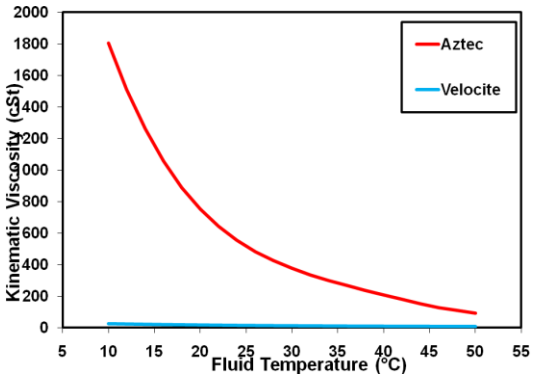

Figure 1 NEL test fluid viscosities

In highly viscous fluids there can be distinguishable variations in the measured temperature due to thermal gradients within the flow path. Thermal gradients are often present in laminar flow due to the parabolic velocity profile that occurs. As there is no mixing taking place between the layers of fluid, the fluid at the centre of the pipe will be at a different temperature than the fluid at the pipe wall. These thermal gradients can make it problematic to obtain a suitably representative mean fluid temperature. This increases the uncertainty of any temperature based correction applied by the device.

The velocity profile of the fluid is also considerably altered by changes in the fluid viscosity. The influence that fluid viscosity exerts on the velocity profile is best defined using the Reynolds number (Re), the dimensionless ratio of inertial forces to viscous forces in a flowing fluid. Reynolds number can be written as:

$$\mathrm{Re} = \frac{U\,D}{\nu} \qquad (1)$$

Where:

U = Average fluid velocity [m/s] D = Pipe diameter [m]

υ = Kinematic Viscosity [m²/s]

A flowing fluid travels in one of three different flow regimes. Low viscosity fluids travelling at moderate velocities would normally have a high Reynolds number (greater than ~10,000), leading to turbulent flow (Figure 2a). In this regime dynamic forces dominate and the motion is parallel to the pipe axis with mixing occurring

Figure 2 (a) turbulent and (b) laminar flow conditions

between the different layers. When the Reynolds number is low (less than ~2,000) the flow is laminar (Figure 2b). In this regime viscous forces dominate and there is no mixing between the layers. The regime between laminar and turbulent flow is described as 'transitional' and can be extremely unpredictable. The flow quickly switches back and forth between laminar and turbulent behaviour and can cause significant flow measurement challenges.

The flow regime has a direct impact on the shape of the flow profile within the pipe. The velocity profile defines how quickly the liquid is travelling at various points across the cross section of the pipe. Fully developed velocity profiles for laminar and turbulent flow are shown in Figure 3.

In laminar flow, viscous forces dominate causing substantial friction against the pipe wall and the fluid. This results in drag between the layers of the fluid with the fluid velocity gradually increasing from the pipe wall to the centre. The maximum velocity at the centre of the pipe can be approximately twice the average velocity of the flow which results in a velocity profile that is parabolic in shape.

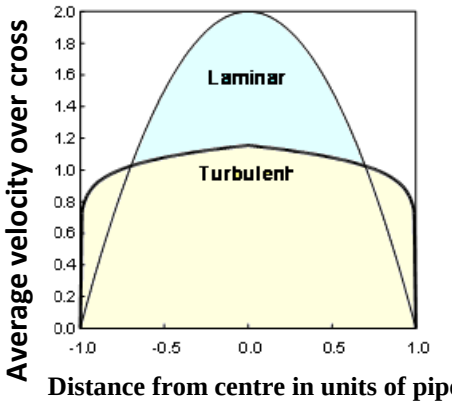

Figure 3 Velocity Profiles

In turbulent flow, the mixing action caused by the dynamic forces breaks up any gradual transfer of drag from the pipe wall. This results in a well-mixed flow with a relatively flat velocity profile. The central axis of fully developed turbulent flow normally has a value of 1.1 to 1.3 times the average flow velocity.

2.2 Scope of Current Work

The effect that medium fluid viscosities have on the current generation of liquid flowmeters (Coriolis, ultrasonic and turbine) has already been reported [1] [2]. However the effect of high viscosity fluids (> 300 cSt) on conventional flowmeters has not yet been defined with independent and verifiable test data. This follows partly from the

scarcity of suitable test facilities capable of providing viscous flow in combination with accurate and traceable reference instrumentation.

The scope of work for the test programme was to explore the performance of conventional flowmeters at elevated liquid viscosities (> 100 cSt). The investigations reported in this paper focus on the performance of differential pressure devices, Coriolis devices and ultrasonic flowmeters. This paper also includes computational fluid dynamics (CFD) results for the two 8 inch Venturi flowmeters evaluated.

3 TEST METERS

3.1 Test Meter Descriptions

The flowmeters evaluated in this test programme ranged from nominally 6 - 8 inch (152.4 – 202.72 mm). This project was not structured as an evaluation of any particular manufacturer or flowmeter model, but rather as a generic evaluation of some of the effects of high viscosity on conventional flowmeter technology. As such, the manufacturer of the flowmeters evaluated in this programme will not be named. The specifications of the flowmeters evaluated are detailed in Table 2.

Table 2 – Test Meter Specifications

Meter	Test Package	Meter Type	Characteristics		
A	2	Venturi	Nominal size Internal diameter (entry pipe) Throat diameter	: : :	8-inch, β = 0.4 202.72 mm 81.10 mm
B	2	Venturi	Nominal size Internal diameter (entry pipe) Throat diameter	: : :	8-inch, β = 0.6 202.72 mm 121.64 mm
C	5	Quadrant edge orifice plate	Nominal size Internal diameter (entry pipe) Throat diameter	: : :	8-inch β = 0.45 193.8 mm 91.44 mm
D	5	Quadrant edge orifice plate	Nominal size Internal diameter (entry pipe) Throat diameter	: : :	8-inch β = 0.6 193.8 mm 121.92 mm
E	1	Ultrasonic	Nominal size Flowrate range (approx.) Internal diameter (entry pipe)	: : :	6-inch 11 to 227 l/s 152.4 mm
F	3	Ultrasonic	Nominal size Recommended Reynolds range Internal diameter (entry pipe)	: : :	6-inch > 10 000 152.4 mm
G	4	Ultrasonic	Nominal size Flowrate range (approx.) Internal diameter (entry pipe)	: : :	6-inch 20 to 200 l/s 150 mm
H	1	Twin tube Coriolis	Nominal size Maximum flowrate (approx.) Internal diameter (entry pipe)	: : :	6-inch 222 kg/s 152.4 mm
I	3	Twin tube Coriolis	Nominal size Maximum flowrate (approx.) Internal diameter (entry pipe)	: : :	6-inch 250 kg/s 152.4 mm

3.2 Differential Pressure Devices – Venturi & Quadrant Edge Orifice Plate

Differential pressure (DP) devices are a well established flow metering technology and have been used in industry for decades. Many new flow metering technologies have been developed in recent years, but differential pressure devices are still utilised for flow measurement applications across the world.

This is because differential pressure devices are relatively simple and inexpensive to construct, contain no moving parts and thus require very little maintenance. They can be used in any orientation and are suitable for use in most liquids and gases. There is a large amount of experience using these devices and their performance is well documented. Certain differential pressure devices can be used without calibration by calculating the discharge coefficient using the ISO 5167-1 standard [3].

However, the standard does not present discharge coefficients for Reynolds numbers below 5,000 for orifice plates and 20,000 for Venturi tubes and numerous experimental studies have shown a logarithmic relationship between Reynolds number and discharge coefficient in laminar flows. As such, it is expected that traditional DP devices will encounter significant errors when used in highly viscous fluids.

As the ISO 5167 standard only includes limited data for Reynolds numbers down to 50000, we must slightly alter the standard equation by removing the discharge coefficient. Thus, the mass flowrate can be calculated using the following equation:

$$Q_T = A_t \cdot \sqrt{\frac{2 \cdot \Delta P \cdot \rho_{fluid}}{1 - \beta^4}} \tag{2}$$

The discharge coefficient can be calculated by dividing the reference mass flowrate by the calculated mass flowrate.

$$C_D = \frac{Q_{ref}}{Q_T} \tag{3}$$

Where:

ΔP	=	Dynamic Pressure Drop	ρ_{fluid}	=	Fluid Density
A_t	=	Throat Area	C_D	=	Discharge Coefficient
β	=	Diameter Ratio (throat ÷ pipe)			

Quadrant edge orifice plates are believed to be more suitable for high viscosity applications than standard orifice plates. The inlet edges of quadrant edge orifice plates are rounded to quarter circles, which reduces pressure drop across the plate. Quadrant edge orifice plates have higher discharge coefficients than standard concentric edge types (typically 0.8 and 0.6 respectively for turbulent flows). Unlike concentric orifice plates, quadrant edge devices are known for producing near-constant discharge coefficients at very low Reynolds numbers. Thus in theory they should be suitable for high viscosity flow applications.

Figure 4 8 inch β 0.6 Quadrant Edge Orifice Plate Inlet

ISO 5167-2[4] provides discharge coefficients for orifice plates with various pressure tapping locations, but does not provide guidance for quadrant edge orifice plates. There are various sources that can provide estimates for quadrant edge discharge coefficients despite the lack of an international standard.

The Shell Flowmeter Engineering Handbook presents the following equation for quadrant edge orifice plates where discharge coefficient is a function of Beta (β)[5].

$$C_D = 0.73823 + 0.3309\beta - 1.1615\beta^2 + 1.5084\beta^3 \quad (4)$$

The equation has a stated uncertainty of ±2.00 % for Beta ratios greater than 0.316. With the experimental data collected for these orifice plates, the predicted discharge coefficient has been calculated and plotted on the graphs with 2.00 % uncertainty bands.

One of the main advancements in flow measurement in the last five years has been the introduction of the Prognosis [6] measurement system by DP Diagnostics. One of the main advantages of the Prognosis system is its simplicity. It utilises two additional differential pressure measurements across the DP meter and can be explained in more detail below.

Figure 5 shows a generic DP meter with a third pressure tap allowing the traditional DP (ΔP_t), a recovered DP (ΔP_r), and a permanent pressure loss DP (ΔP_{ppl}) to be read. This allows a full patented generic DP meter diagnostic suite to be available.

The sum of ΔP_r and ΔP_{ppl} *must* equal ΔP_t (equation 5). This fact allows a DP reading check. Each DP offers an independent flowrate prediction, i.e. the traditional DP meter flowrate prediction (equation 6), the expansion DP meter flowrate prediction (equation 7), and the PPL DP meter flowrate prediction (equation 8).

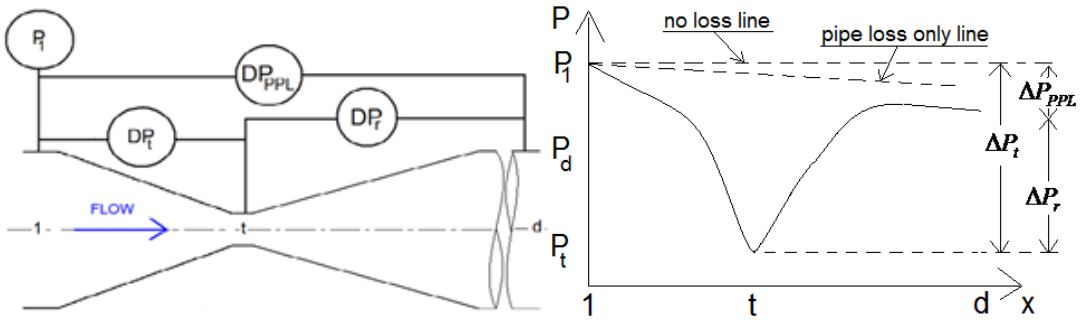

Figure 5 Venturi meter instrumentation sketch and pressure fluctuation graph

$$\Delta P_t = \Delta P_r + \Delta P_{PPL} \quad \text{uncertainty} \pm \theta\% \quad (5)$$

Traditional Flow Equation: $$m = EA_t C_d \sqrt{2\rho\Delta P_t} \quad \text{uncertainty} \pm x\% \quad (6)$$

Expansion Flow Equation: $$m = EA_t K_r \sqrt{2\rho\Delta P_r} \quad \text{uncertainty} \pm y\% \quad (7)$$

PPL Flow Equation: $$m = AK_{ppl} \sqrt{2\rho\Delta P_{PPL}} \quad \text{uncertainty} \pm z\% \quad (8)$$

These three flowrate predictions can be compared. The percentage difference between any two flowrate predictions should not be greater than the root mean square of the two flowrate prediction uncertainties. Table 3 displays the flowrate predictions.

Table 3 – Flowrate prediction pair diagnostics

Flow Prediction Pair	% Actual Difference	% Allowed Difference	Diagnostic Check
Traditional & PPL	$\phi\%$	$\psi\%$	$-1 \le \psi\%/\phi\% \le +1$
Traditional & Expansion	$\xi\%$	$\lambda\%$	$-1 \le \lambda\%/\xi\% \le +1$
PPL & Expansion	$\upsilon\%$	$\chi\%$	$-1 \le \chi\%/\upsilon\% \le +1$

With three DPs read, there are three DP ratios:

PPL to Traditional DP ratio (PLR): $$(\Delta P_{PPL} / \Delta P_t)_{reference}, \quad \text{uncertainty} \pm a\%$$

Recovered to Traditional DP ratio (PRR): $$(\Delta P_r / \Delta P_t)_{reference}, \quad \text{uncertainty} \pm b\%$$

Recovered to PPL DP ratio (RPR): $$(\Delta P_r / \Delta P_{PPL})_{reference}, \quad \text{uncertainty} \pm c\%$$

A DP meter's DP ratios are characteristics of that meter. DP ratios found in service can be compared to their expected values. The difference between a found and expected value should not be greater than the reference DP ratio uncertainty. Table 4 displays the flowrate prediction pair diagnostics.

Table 4 – DP Ratio diagnostics

DP Ratio	% Actual to Ref Difference	% Reference Uncertainty	Diagnostic Check
PLR	$\alpha\%$	$a\%$	$-1 \le \alpha\%/a\% \le +1$
PRR	$\gamma\%$	$b\%$	$-1 \le \gamma\%/b\% \le +1$
RPR	$\eta\%$	$c\%$	$-1 \le \eta\%/c\% \le +1$

Any inference that Equation 5 does not hold is a statement that there is a malfunction in one or more of the DP transmitters. The sum of ΔP_r and ΔP_{ppl} gives an 'inferred' $\Delta P_{t,inf}$. The inferred and directly read traditional DP should not be greater than the root mean square of the combined DP transmitter uncertainties. Table 5 displays the DP reading integrity diagnostics.

Table 5 – DP Reading Integrity Diagnostic

% Actual to Inferred Traditional DP Difference	% RMS Combined DP Reading Uncertainty	Diagnostic Check
$\delta\%$	$\theta\%$	$-1 \le \delta\%/\theta\% \le +1$

Table 6 displays the seven possible situations where these diagnostic would signal a warning. For convenience we use the following naming convention:

Normalized flowrate inter-comparisons: $x_1 = \psi\%/\phi\%$, $x_2 = \lambda\%/\xi\%$, $x_3 = \chi\%/\upsilon\%$

Normalized DP ratio comparisons: $y_1 = \alpha\%/a\%$, $y_2 = \gamma\%/b\%$, $y_3 = \eta\%/c\%$

Normalized DP sum comparison: $x_4 = \delta\%/\theta\%$

Table 6 – The DP meter possible diagnostic results

DP Pair	No Warning	WARNING	No Warning	WARNING
ΔP_t & ΔP_{ppl}	$-1 \le x_1 \le 1$	$-1 < x_1$ or $x_1 > 1$	$1 \le y_1 \le 1$	$-1 < y_1$ or $y_1 > 1$
ΔP_t & ΔP_r	$-1 \le x_2 \le 1$	$-1 < x_2$ or $x_2 > 1$	$1 \le y_2 \le 1$	$-1 < y_2$ or $y_2 > 1$
ΔP_r & ΔP_{ppl}	$-1 \le x_3 \le 1$	$-1 < x_3$ or $x_3 > 1$	$1 \le y_3 \le 1$	$-1 < y_3$ or $y_3 > 1$
$\Delta P_{t,read}$ & $\Delta P_{t,\inf}$	$-1 \le x_4 \le 1$	$-1 < x_4$ or $x_4 > 1$	N/A	N/A

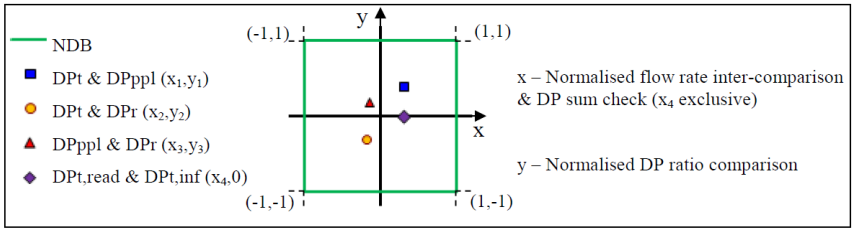

Figure 6 Normalized diagnostic box (NDB) with diagnostic results & DP check

For practical use, a graphical representation is simple and effective. A box is drawn centred on a graph's origin. Four points are plotted representing the seven diagnostic checks (Figure 6). If the meter is fully serviceable all points must be inside the box. One or more points outside the box indicate a malfunction. The diagnostic pattern of an alarm offers information on the source of the malfunction. Different malfunctions can cause different patterns. Steven et al [6] gives a review of these diagnostics.

3.3 Coriolis

Coriolis flowmeters provide a direct measurement of mass flowrate and product density with stated uncertainties as low as 0.1% and 0.05 kg/m^3 respectively for light hydrocarbons. Advantages such as high accuracy, claimed insensitivity to installation and direct measurement of mass flow have led to wide scale adoption across a number of sectors, including the food, pharmaceutical and process industries.

Figure 7 Examples of Coriolis Flow Tube Configurations

Coriolis manufacturers have previously claimed to have negligible sensitivity to increasing fluid viscosity. Some manufacturers now accept that Coriolis devices have a sensitivity to flow profile / low Reynolds numbers with viscous fluids [7].

Coriolis meters are prone to "zero offset" errors, and so the meters were zeroed when first installed in the test line, and after each temperature change. The Coriolis devices were evaluated under these conditions for the duration of the test programme.

The performance of Coriolis flowmeters is detailed in the ISO standard 10790 [8]. However, the performance of Coriolis meters in high viscosity fluids and the potential adverse effect of flow profile / low Reynolds numbers are not addressed.

3.4 Ultrasonic

Ultrasonic flowmeters are currently employed in a variety of custody transfer and allocation measurement systems for conventional "light" oils. They have been known to achieve measurement uncertainties of better than ±0.15 % over most of their turndown range. However, one property that may adversely affect the performance of these meters is the variation in velocity profile that occurs with pipe Re number.

To maintain an accurate estimate for volumetric flowrate, ultrasonic meters must reliably determine the mean fluid velocity from discrete measurements of fluid velocity along the ultrasonic paths. Many manufacturers will apply corrections to the meters for the velocity profile of the flow.

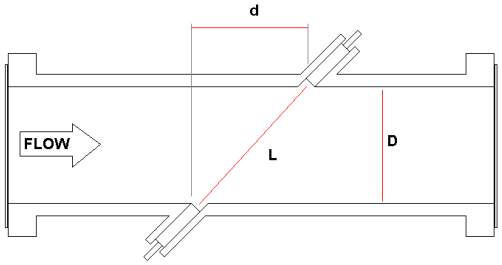

Figure 8 Typical In-Line USM Transducer Set Up

Depending on the transducer frequency employed by the ultrasonic device, high viscosity fluids can cause signal attenuation. This could potentially lead to substantial errors in the measurement of the flow due to less "successful" measurements of the flow velocity being recorded by the device. By utilising the signal diagnostics from the ultrasonic device, it's possible to ascertain whether signal attenuation has occurred.

Full bore ultrasonic meters introduce no additional pressure drop compared to a standard straight length of pipe. This may be of particular advantage over other meter types for use in high viscosity fluids where pressure drops are considerably large. However some manufacturers specify that their device should be installed with a flow conditioner and 10 diameters of straight pipe lengths upstream and 5 diameters downstream. Depending on the fluid viscosity and velocity, this could potentially be a sizeable additional pressure drop. This could be a key consideration in high viscosity applications.

The ISO standard for ultrasonic devices, ISO 12242, does not cover in depth the effect that fluid viscosity and fluid Reynolds number has on the performance of ultrasonic devices [9].

4 EXPERIMENTAL PROGRAMME

4.1 Oil Flow Facility

The experimental programme was completed in 2012 at the UK National Standards Oil Flow Facility, located at NEL in Glasgow, Scotland. The facility consists of two separate flow circuits (A and B), each with a high capacity and a low capacity flow line. These can accommodate nominal pipe sizes from 0.5" to 10", and can operate at line pressures up to 10 bar. Test fluids can be delivered at flowrates up to 720 m^3/hr. Six test fluids are available in this facility – Kerosene, Gas Oil, Velocite, Primol, Siptech and Aztec – covering liquid viscosities from 2 to 1500 cSt. Figure 9 displays the kinematic viscosity of NEL's test fluids for the Oil Flow Facility in 2013.

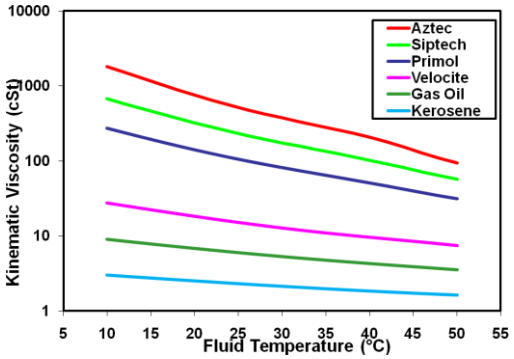

Figure 9 Kin. Viscosity of NEL test fluids

Figure 10 shows a schematic diagram of the flow circuits. The oil for each circuit is drawn from a 30 m^3 supply tank, from where it is discharged to the test lines. A conditioning circuit, linked to each tank, maintains the oil temperature to within ± 0.5 ºC of a pre-selected value (itself set in the range 10 – 50 ºC).

Line temperature and pressure are monitored both upstream and downstream of the test section. The flow lines share a common primary standard weighbridge system consisting of four separate weigh tanks of 150, 600, 1500 and 6000 kg capacity. The facility is fully traceable to National Standards and is accredited by the United Kingdom Accreditation Service (UKAS) to ISO 17025.

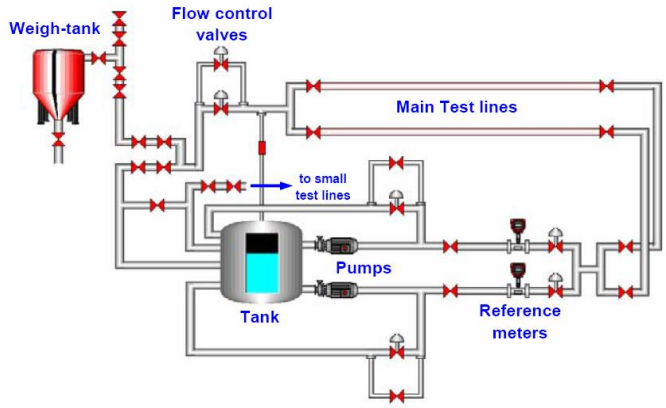

Figure 10 Schematic diagram of the NEL oil flow test facility

4.2 Reference System

For "primary" calibrations, a gravimetric "standing-start-and-finish" method is used to determine the quantity of fluid (volume or mass) which has passed through the flowmeter under test and into the selected weigh tank. The gravimetric weigh tanks constitute the primary reference standard of the NEL oil flow facility. Using the above technique, the overall uncertainty in the quantity of fluid passed, expressed at the 95% confidence limit is ± 0.03 % (k = 2). For a "secondary" calibration, the quantity of oil passing through the test meter is measured using a pre-calibrated reference meter, installed in series. The reference meters used at NEL have a history of previous calibrations and typical uncertainties in the quantity of fluid passed of the order of ± 0.08 % (k = 2). This applies to oils with a kinematic viscosity between 2 – 30 cSt.

In the evaluation programme the oil flow facility was operated in 're-circulation' mode and the test meter compared against secondary reference standards. The reference meters used in the present test programme consisted of two 8-inch rotating-vane Positive Displacement device. The "K-factor" for this type of PD meter can be considered to be a function of three main parameters: the volumetric flowrate (Q), the liquid viscosity (ν) and the fluid temperature (T).

The PD meters were calibrated (as a function of flowrate only) for the fluid temperature and fluid type detailed in the test matrix. This provided the most accurate reference for testing and produced a K-factor curve of the form:

$$K_{F,T} = f_{F,T}(Q) \tag{5}$$

Where F and T denote the fluid type or test temperature respectively. The resultant uncertainty of the PD meters in service was of the order of ± 0.15% at the 95% confidence level.

4.3 Test Matrix

To investigate the sensitivity of the flowmeters to elevated fluid viscosity, a series of tests were made on the flowmeters at a controlled and monitored rate. The test installations were based around standard pipeline runs of 6 or 8-inch nominal bore depending on the flowmeter dimensions. Tests were conducted at a range of flowrates using Aztec as the test fluid. The nominal viscosity range covered was 100 – 1500 cSt.

To enable the effects of elevated viscosity to be evaluated, the nominal test matrix of Table 7 was proposed. Figure 11 displays the corresponding pipe Reynolds numbers covered in the test programme.

Table 7 – Nominal Test Matrix

Fluid	Temperature (°C)	Kin. Viscosity (°C)	Flowrate (l/s)	
			Min	Max
Aztec	12 - 45	1500 - 100	10	130

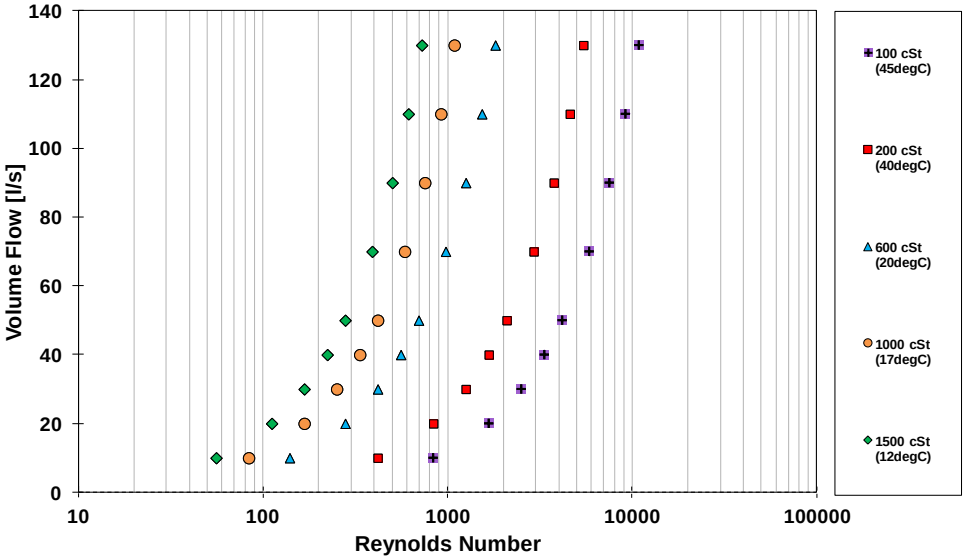

Figure 11 Range of Pipe Reynolds numbers Covered by Test Matrix

5 TEST RESULTS

The test programme was completed in 2012 independently by NEL. The flowmeter manufacturers were involved in setting up their own devices but did not influence the test programme.

It should be noted that the test results are for high viscosity flow measurement using conventional liquid flowmeters. This remains a problematic area for flow measurement technologies and improving the uncertainty in this area requires further investigation.

Differential Pressure Devices – Venturi Tubes

Meter A – 8" β = 0.4

The experimentally measured discharge coefficients for the Venturi are shown in Figure 12 below. The calculated discharge coefficients were plotted against the throat Reynolds number for a variety of temperatures, viscosities and flowrates, and were all found to lie on a single curve.

The discharge coefficient conforms to what is described in ISO 5167-4 [10] and increases with Reynolds number. The trend tends towards horizontal as it moves into the turbulent regime. Data points from the full range of viscosities form a single, well defined curve. The minimum discharge coefficient observed is 0.638 at a Reynolds number of 114. The maximum is 0.955 at a Reynolds number of 20568.

It is important to note that Reynolds numbers are plotted on a logarithmic scale, and it can be seen that very sharp changes in discharge coefficient occur with only small changes in Re in the laminar region.

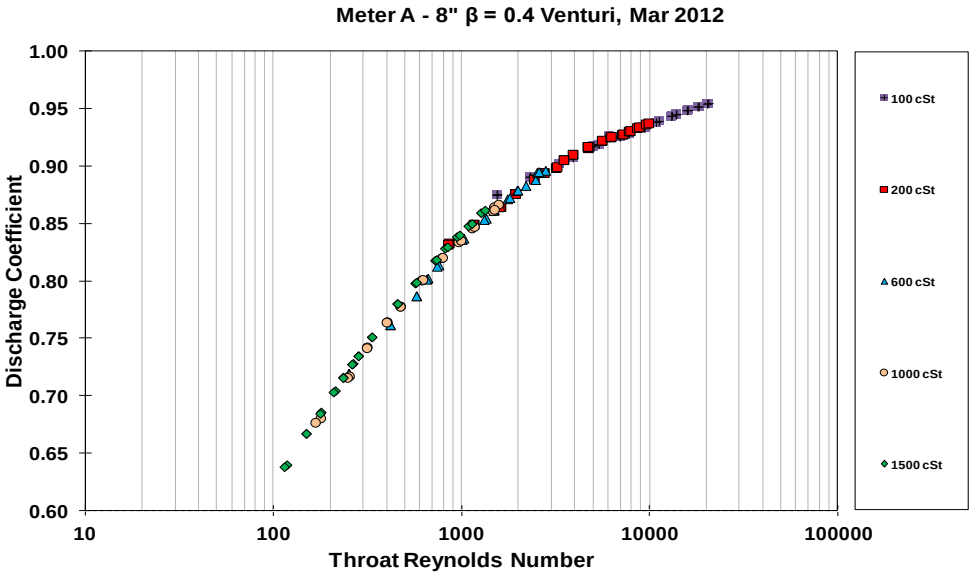

Figure 12 Venturi A – Discharge Coefficient vs. Throat Reynolds number

Meter B – 8" β = 0.6

The discharge coefficient curve for Meter B is well defined with data series from the full range of viscosities overlapping closely. Changes in discharge coefficient are very sudden at low Reynolds numbers but the curve tends towards horizontal as it moves towards the turbulent regime.

Unlike Meter A, the data for Meter B features a small "hump" at Reynolds numbers of approximately 2000. Literature sources typically describe discharge coefficient trends for Venturi tubes as smooth curves with no mention of a "hump" in this range, but this is a feature that has been observed previously at NEL [11] and by others [12] [13]. The minimum discharge coefficient observed is 0.625 at a Reynolds number of 116. The maximum is 0.951 at a Reynolds number of 15280.

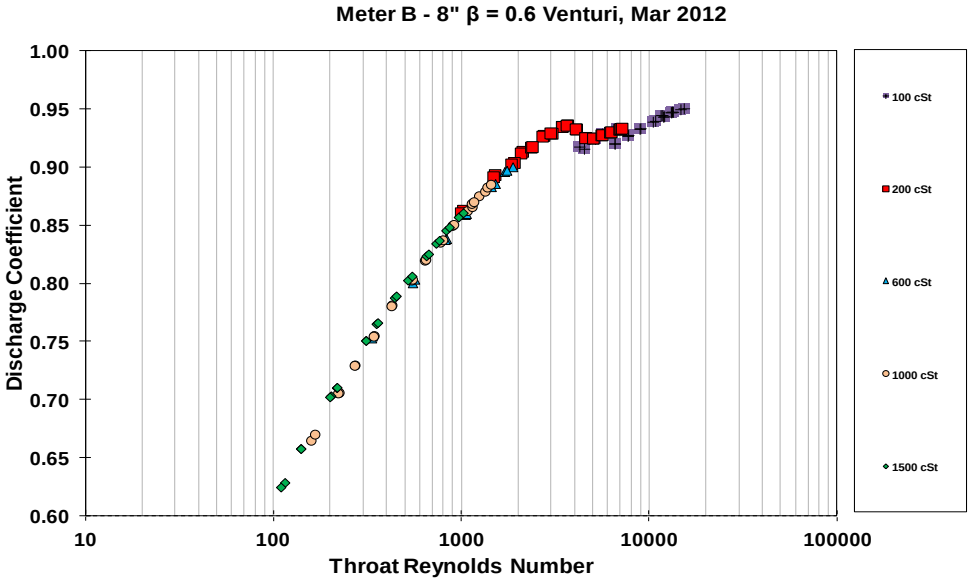

Figure 13 Venturi B – Discharge Coefficient vs. Throat Reynolds number

The discharge coefficient curves for Meter A and Meter B are compared in Figure 14. It can be seen that at higher Reynolds numbers, there is little difference in discharge coefficients between the two Venturi tubes. Meter A has a discharge coefficient of 0.955 at Re_T = 20568 and Meter B has a discharge coefficient of 0.951 at Re_T = 15280.

As mentioned previously, a "hump" is observed for Meter B but not for Meter A. This is likely because the smaller internal diameter of Meter A has a conditioning effect on the flow, causing the flow regime to shift from laminar to turbulent more suddenly.

Meters A and B conform to the ISO 5167-4 [10] definition of "Classical Venturi tube with a machined convergent section". A steady discharge coefficient of 0.995 should be achieved for Reynolds numbers in the range $2 \times 10^5 \leq Re \leq 1 \times 10^6$. However, the guidelines in the standard do not apply to heavy oils operating predominantly in the laminar and transitional flow regime.

The classic definitions for laminar and turbulent flow are Re < 2000 and Re > 4000 respectively, with transitional flow occurring between the two regimes. However, it is also acknowledged that the transition point can occur at higher Reynolds and can be influenced by upstream installation conditions, pipe incline and surface roughness.

At Re_T = 5000 both Venturi tubes showed discharge coefficients of approximately 0.93. If compared to the discharge coefficient of 0.995 stated in the standard, this represents a flow error of greater than 6.5 %. At Re = 1000, flow error would be greater than 9.5%.

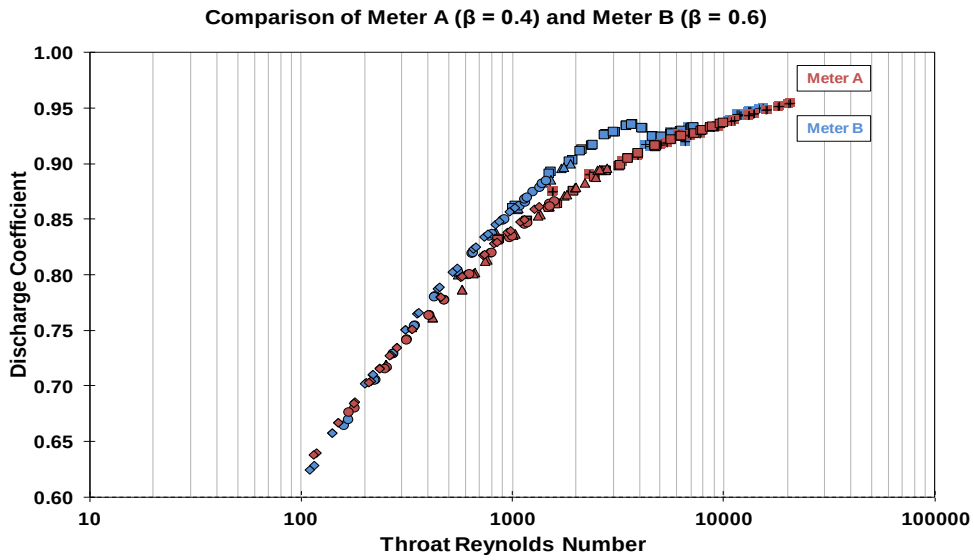

Figure 14 Comparison of Venturi Tubes

This study has shown that in the laminar or transition region the measured value of the discharge coefficient deviates significantly from the value given in the standard of 0.995. The possible reasons for this deviation are discussed in the CFD Study completed by NEL.

NEL compared the experimental test results for the two 8 inch Venturi meters to those determined from CFD simulations over a range of flowrates and fluid viscosities. The purpose of the study was to determine the capability of computational fluid dynamics (CFD) to accurately predict the flow of heavy oils through a Venturi meter.

The CFD code, ANSYS FLUENT 13.0 was used to model the flow through two Venturi meters. For simplicity and speed of convergence, the geometry of each Venturi was modelled using a two-dimensional asymmetric domain with a structured grid. The meters correspond to Meter A and Meter B described in the main body of this report. The meters are designed in accordance with the industry standard [10].

Figure 15 and Figure 16 show the modelled and experimentally obtained Venturi discharge coefficient plotted against the Venturi throat Reynolds number for Meter A and Meter B, respectively. Despite investigating oils of varying viscosities and flowrates, both plots show the modelled C_D values falling on a single curve when plotted against throat Reynolds number. This observation is mirrored by that witnessed in the test data. This reinforces the assumption that C_D is a function of throat Reynolds number only. Figure 15 indicates excellent agreement between the CFD simulations and the test data across the complete Reynolds number range examined. The curvature of the trend is predicted very well. With heavy oils, the flow is more often laminar due to the high viscosity; this region on the curve is predicted especially well using the laminar model in Fluent for $Re_T < 2300$.

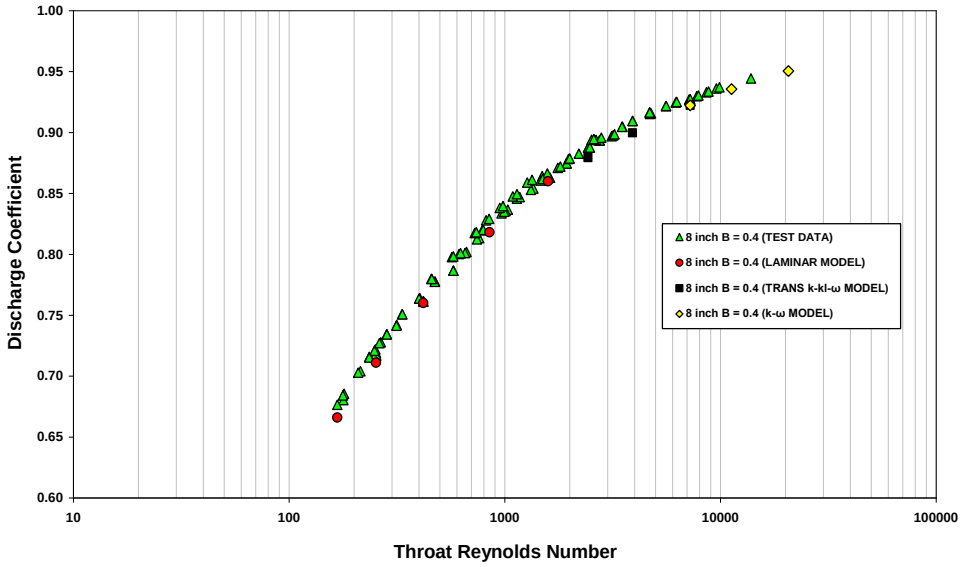

Figure 15 Meter A – Experimental & CFD Results for C_D vs. Re_T

In Figure 16 there is excellent agreement between CFD and the test data up to Re_T = 3449. The model again performs well within the laminar regime expected for most heavy oil flows. At some point above Re_T = 3449, transition to turbulent flow occurs within the boundary layer formed on the pipe wall; this is observed by the sudden decrease in the discharge coefficient, known as the "hump", associated with laminar to turbulent transition occurring through the meter. The *k-kl-ω* transition model accurately predicts the onset of the "hump" at Re_T = 3449; however, the gradient of the "hump" is too severe in comparison to the test data. As a result, C_D values are

under predicted up to Re_T = 6581. At turbulent Reynolds numbers above Re_T = 6581, as the discharge coefficient recovers, the gradient of the CFD data is again slightly more severe than in test data, resulting in over predicted values of C_D.

The presence of a "hump" in the modelled and experimental data for Meter B is suggested in literature to be a result of laminar-turbulent transition occurring through the meter. Shlichting offers an explanation of experimental results on transition from laminar to turbulent flow.

Shlichting observed transition to cause a notable change in the velocity distribution over the pipe cross section [14]. In laminar flow, the velocity distribution over the pipe cross section is parabolic; however, in turbulent flow, the velocity distribution will become more uniform and flat. Figure 17 shows plots of the velocity profile at the Venturi throat pressure tap determined from the CFD simulations of Meter B. The y-axis shows the throat radius where 0 represents the centre of the throat. The velocity profile is shown clearly evolving from a parabolic to flattened shape with increasing throat Reynolds number. Figure 16 shows the "hump" beginning at around Re_T = 3500. Figure 18 shows the difference between the velocity profile at Re_T = 3449 and sometime after at Re_T = 4004, as the discharge coefficient starts to decrease. The abrupt jump from a parabolic to uniform velocity distribution over such a small range of Re_T is indication that transition has occurred.

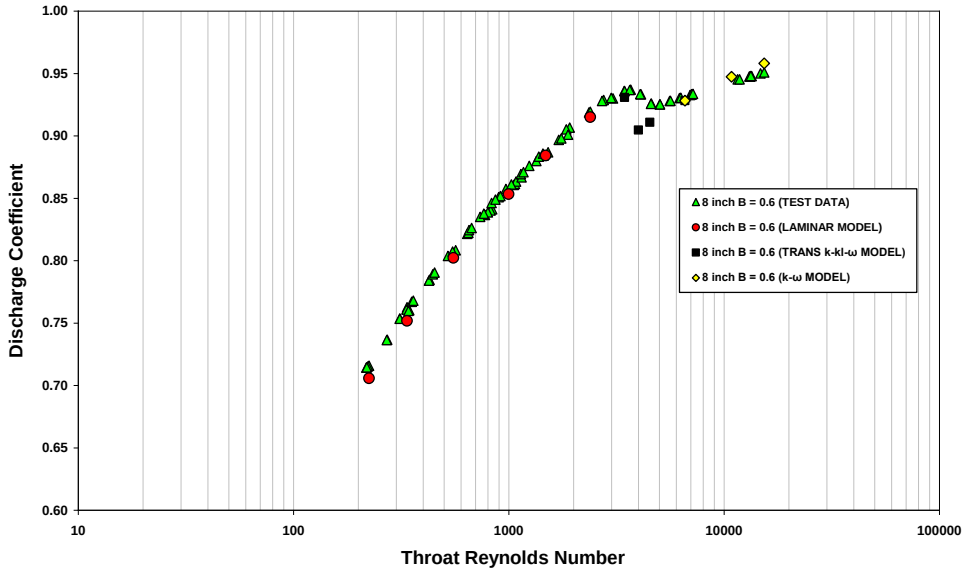

Figure 16 Meter B – Experimental & CFD Results for C_D vs. Re_T

O. Reynolds [15] determined from early investigations that transition from laminar to turbulent flow always takes place at about the same critical Reynolds number, found to be Re_{crit} = 2300. He later stated that the critical Reynolds number can increase as the disturbances in the flow are decreased. The CFD simulations were run assuming a smooth pipe; as both the modelled and experimental data predict the onset to the "hump" at Re_T ~ 3500; this is a good indication that flow disturbances in the flow both leading up to, and through the meter, were minimal during the experiments.

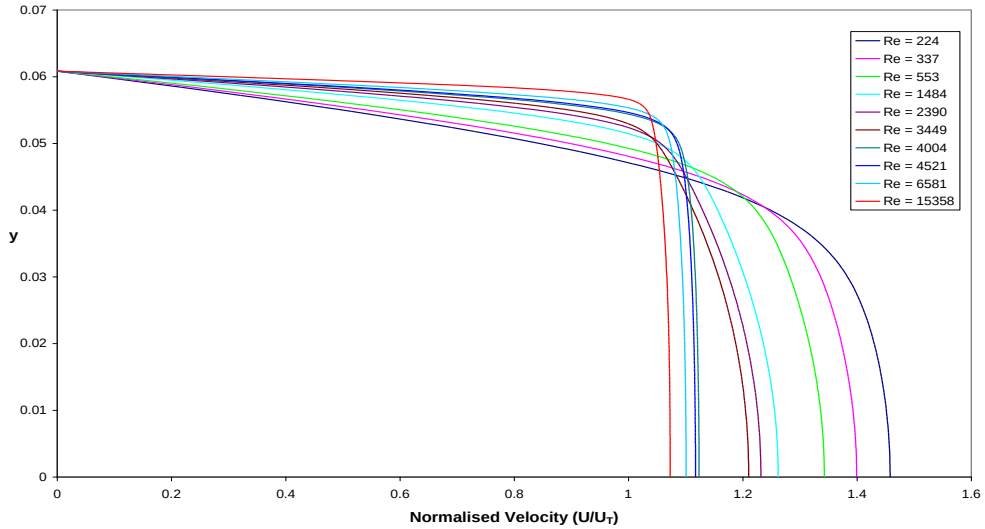

Figure 17 Meter B – Velocity Profiles at the Venturi Throat Pressure Tap over a Range of Throat Reynolds numbers

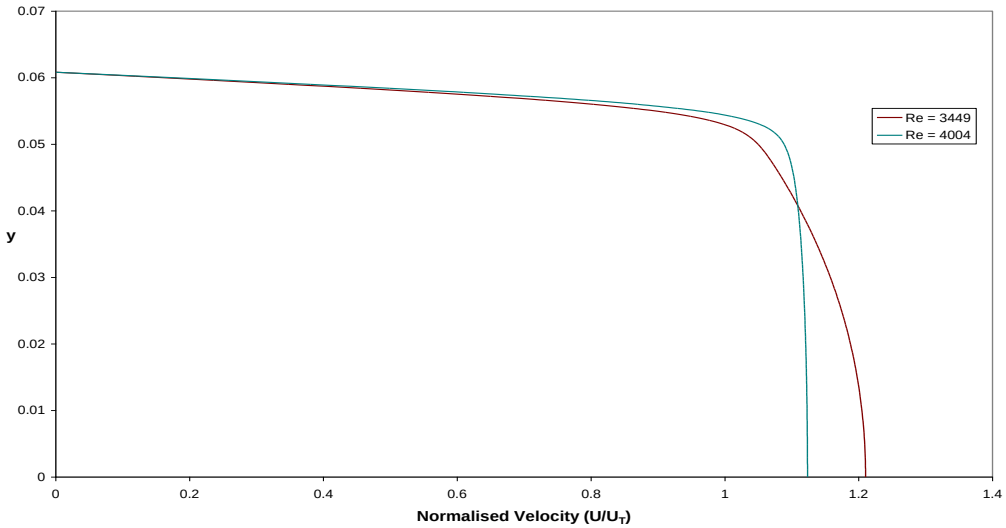

Figure 18 Meter B – Velocity Profiles at the Venturi Throat Pressure Tap at two Throat Reynolds numbers

Shlichting goes on to state that transition from laminar to turbulent flow is accompanied by a large change in the resistance to flow [14]. For flow through pipes this equates to a large change in skin friction. This change in friction has a noticeable influence on the longitudinal pressure gradient and therefore, the Venturi pressure drop. For laminar flow, the longitudinal pressure gradient is proportional to the first power of velocity [14]. In turbulent flow the pressure gradient becomes nearly proportional to the square mean velocity of the flow [14]. This influence on the Venturi pressure drop may explain why the discharge coefficient appears to follow two separate curves in Figure 16: one for laminar flow (Re = 235 to 3500) and one for turbulent flow (Re = 5000 to 10820).

Shlichtings' final observation states that around the transition period there is a sudden increase in the boundary layer thickness [14]; Hall [16] later explained the shape of the Venturi calibration curve by defining the discharge coefficient as being the ratio of the "actual" flow area to the geometrical cross sectional area of the throat. Here he

postulated that the displacement thickness of the boundary layer behaves as a flow reducer that diminishes in its effect with increasing Reynolds number.

Combining these two assumptions, the following attempts to describe the shape of calibration curve for Meter B. As the flow regime becomes increasingly turbulent through the throat, the velocity distribution becomes more and more uniform (flat), decreasing the boundary layer thickness and increasing the "actual" flow area seen by the flow. The reduced effect of the throat to restrict the flow results in an increase in the static pressure at the throat tapping, causing the discharge coefficient to increase with increasing Re_T.

Around transition, the boundary layer thickens suddenly, as postulated by Shlichting, causing the "actual" flow area to reduce, restricting the flow and decreasing the value of C_D. In Figure 16, it has been shown that between Re_T = 3500 and 5000, values of C_D decrease in the experimental data, contributing to the "hump" in the calibration curve. At some point thereafter, accompanied with a change in the friction resistance, the velocity distribution becomes uniform in turbulent flow. Here the "actual" flow area begins to closely approach that of the geometrical cross sectional area of the throat, resulting in a recovery of C_D to values close to unity, as seen in Figure 16.

Differential Pressure Devices – Quadrant Edge Orifice Plates

Meter C – 8" β = 0.45

Data points from the full range of viscosities form a well defined curve with a reasonably tight overlap. The discharge coefficient increases with pipe Reynolds number until a maximum "hump" is reached. The discharge coefficient then drops and becomes linear as Reynolds numbers increase towards the turbulent regime.

The minimum discharge coefficient observed is 0.7554 at a pipe Reynolds number of 139. The maximum C_D is 0.815 at a Reynolds number of 2193. After the "hump" (Re ~ 4000), discharge coefficient is relatively constant at approximately 0.802. The "predicted" discharge coefficient is 0.789, which means that the experimentally determined discharge coefficient has a 1.58 % discrepancy from this reference, which is within the stated 2.00 % uncertainty of the equation. The linearity of the orifice plate in this range is approximately 0.142 %.

It is important to note that the pipe Reynolds numbers are plotted on a logarithmic scale, and so it can be seen that very sharp changes in discharge coefficient occur with only small changes in Re in the laminar region. There are also very sharp changes in the transitional region due to the "hump".

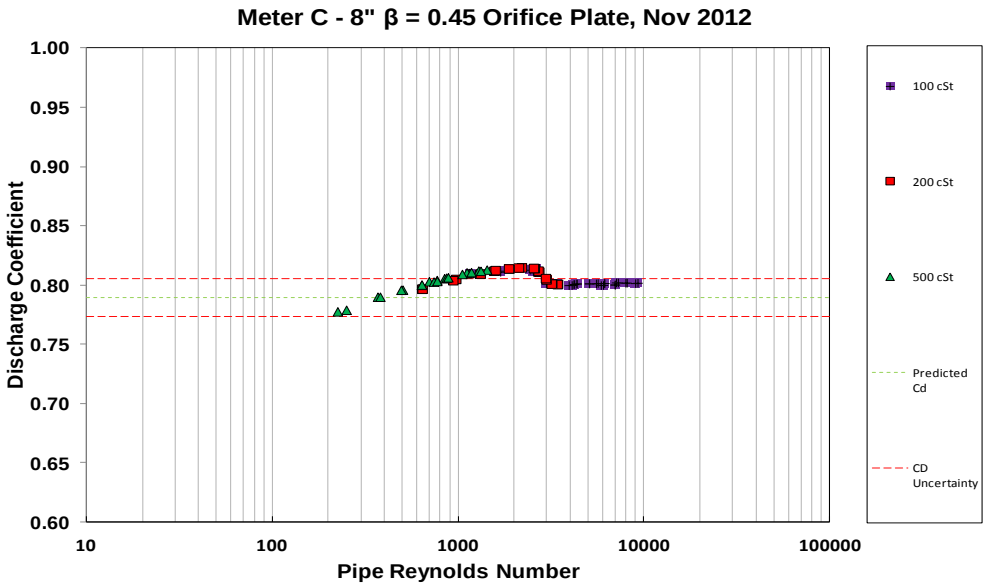

Figure 19 Orifice Plate C – Discharge Coefficient vs. Reynolds number

Meter D – 8" β = 0.6

Data points from the full range of viscosities form a well defined curve with very tight overlap. The discharge coefficient increases with Reynolds number until a maximum "hump" is reached. The discharge coefficient then drops and becomes linear as Reynolds numbers increase towards the turbulent region.

The minimum discharge coefficient observed is 0.7566 at a Reynolds number of 82. The maximum is 0.8782 at a Reynolds number of 1832. After the "hump" (Re ~ 4000), discharge coefficient is relatively constant at approximately 0.8373. The "predicted" discharge coefficient is 0.844, which means that the experimentally determined discharge coefficient has a 0.794 % discrepancy from this reference, which is within the 2.00 % uncertainty of the equation. The linearity of the orifice plate in this range is approximately 0.078 %.

Meter D features a greater beta ratio than Meter C, and it is known that a greater throat bore increases the height of the discharge coefficient curve "hump" [21].

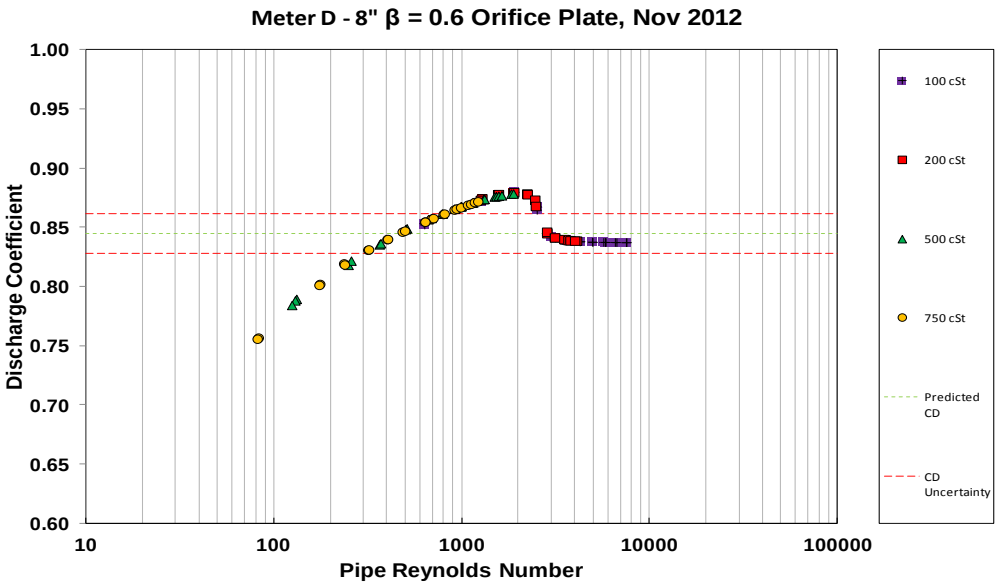

Figure 20 Orifice Plate D – Discharge Coefficient vs. Reynolds number

The discharge coefficient curves for both orifice plates are displayed in Figure 21. Meters C and D show the same general trend, but Meter D displays greater discharge coefficients overall (maximum of 0.8782 compared to 0.8147) and at near turbulent conditions (0.8373 compared to 0.8015). Meter D also displays a linear discharge coefficient for $4000 \leq Re \leq 10000$.

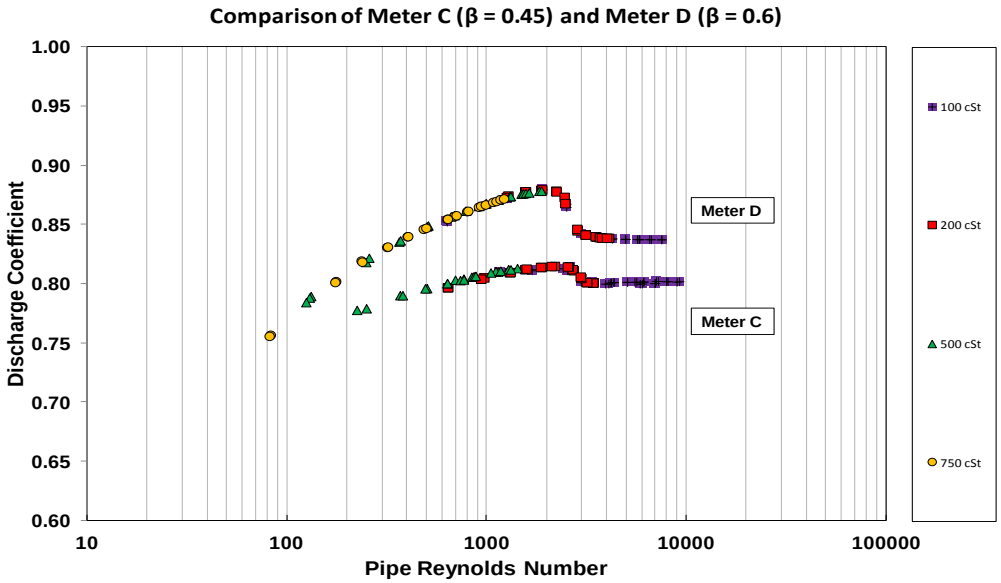

Figure 21 Comparison of Quadrant Edge Orifice Plates

Ultrasonic Flowmeters

Meter E

Meter E was equipped with a 6-inch tube bundle with 10 diameters of straight pipe upstream. The device was originally operated uncorrected. The volumetric flow errors are plotted against reference flowrate in Figure 22.

The uncorrected results for Meter E display moderately high errors, with a maximum of approximately 3%. Two distinct trends can be observed; errors are greater at higher viscosities, and at lower flowrates.

The greatest errors occur for the 1500 cSt tests, and the minimum for the 200 cSt tests. At low flowrates the errors range from 1–3%, and at higher flowrates they range from approximately 1–2 %. As the flowrates increase, the influence of viscosity on errors becomes less prominent. The greatest errors are still found in the 1500 cSt data series, but the smallest errors are found for one of the 600 cSt series rather than the 200 cSt.

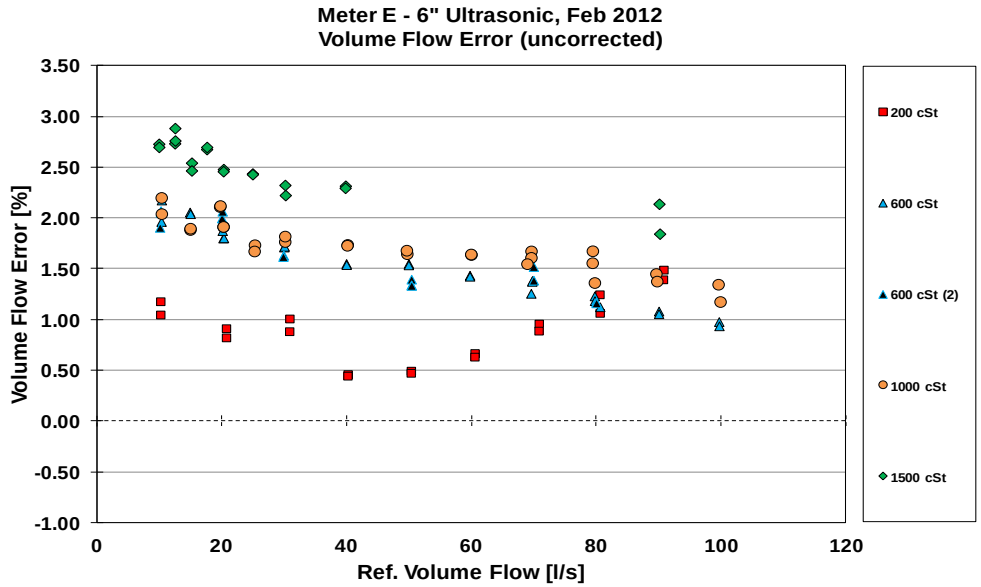

Figure 22 Ultrasonic E – Vol. Flow Error vs. Vol. Flow

Errors from the uncorrected data form a clearer trend when plotted against Reynolds number, as seen in Figure 23. The trends for viscosity and flowrate can be observed as a Reynolds number effect. As Reynolds number decreases, error increases sharply. Above Re ~ 2000, errors increase. It is likely that this sudden increase in error is due to the transition region where the flow regime changes from laminar to turbulent.

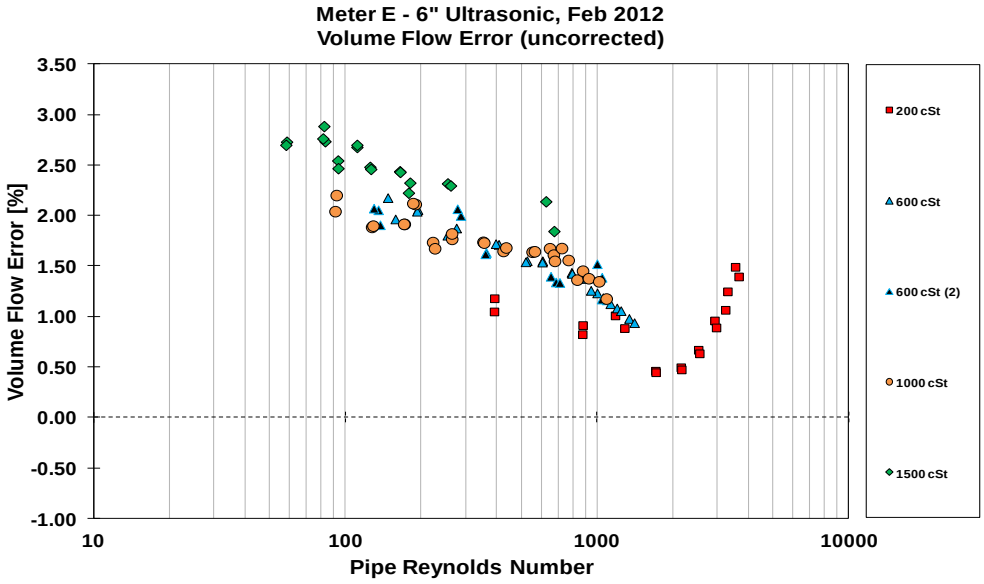

Figure 23 Ultrasonic E – Vol. Flow Error vs. Reynolds number

A second set of test data was taken for Meter E, this time with a flowrate-based correction applied to the meter. A different correction factor was used for each viscosity and the resulting volumetric flow errors are plotted in Figure 24.

The corrected data shows significant improvement over uncorrected, the maximum error is 1.209% and for most of the range, it is less than 0.5%. Unlike the uncorrected data, the greatest errors occur at the higher flowrates, which is unusual for an ultrasonic flowmeter. This is likely due to the fact that the correction applied was a third order polynomial or greater and is under-compensating at high flowrates as a result of the inflection point of the polynomial curve.

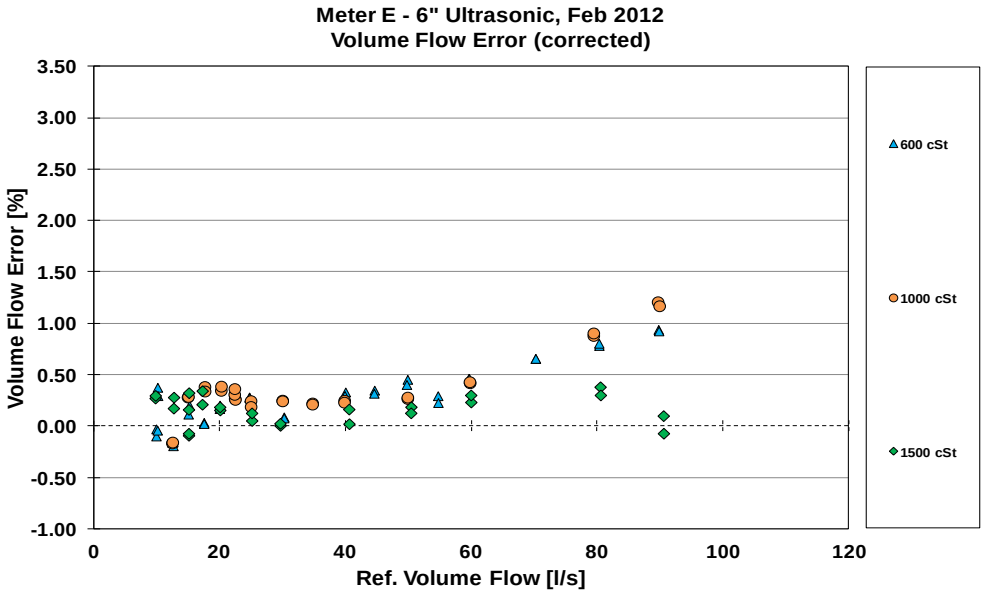

Figure 24 Ultrasonic E – Vol. Flow Error vs. Vol. Flow (corrected)

The corrected data for meter E was plotted against Reynolds number in Figure 25. The greatest errors occur at Reynolds numbers less than 100 and at approximately 1000. The smallest errors occur for Reynolds numbers between 100 to 500.

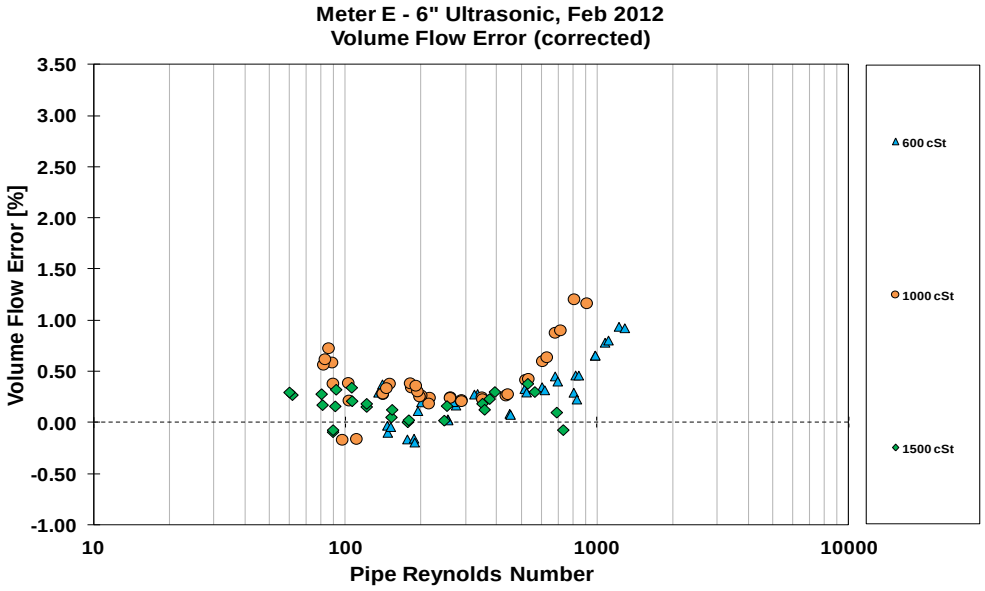

Figure 25 Ultrasonic E – Vol. Flow Error vs. Reynolds number (corrected)

Meter F

The vendor for Meter F decided the device should not be installed with a flow conditioner. However, 30 diameters of straight pipe were in place immediately upstream of the meter. The volumetric flow errors for Meter F are plotted against reference flowrate in Figure 26. The meter was operated with no correction applied to the device throughout the tests.

The meter shows spurious readings with lots of scatter for the 1000 cSt test condition. This effect may be due to signal attenuation at the higher viscosity. The errors are more negative at low flowrates and more positive at higher flowrates and range from -8.35 to 4.5 % for this series.

Although the 1000 cSt readings are highly scattered, the greatest error for the 200 cSt and 600 cSt tests is -1.335%. The majority of the 200 cSt and 600 cSt data points are within ±1 % error. Similar to the 1000 cSt series, errors are more negative at low flowrates and more positive at high flowrate for these two series, although the trend is less pronounced.

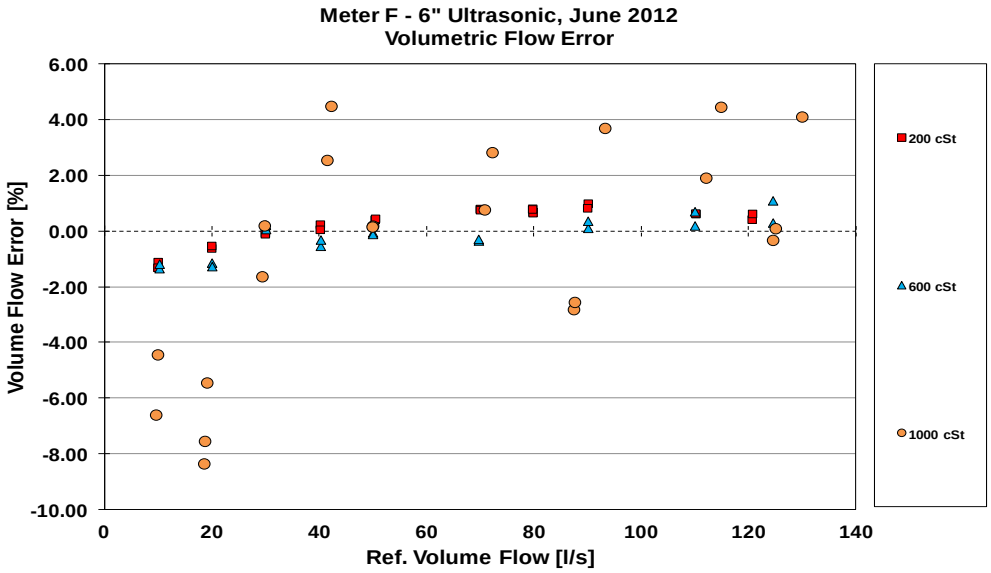

Figure 26 Ultrasonic F – Vol. Flow Error vs. Vol. Flow

The error data for Meter F is plotted against Reynolds number in Figure 27 and shows a tendency for Meter F to under-read at low Reynolds numbers. The 200 cSt data appears to display a positive bias at Reynolds numbers greater than 2000.

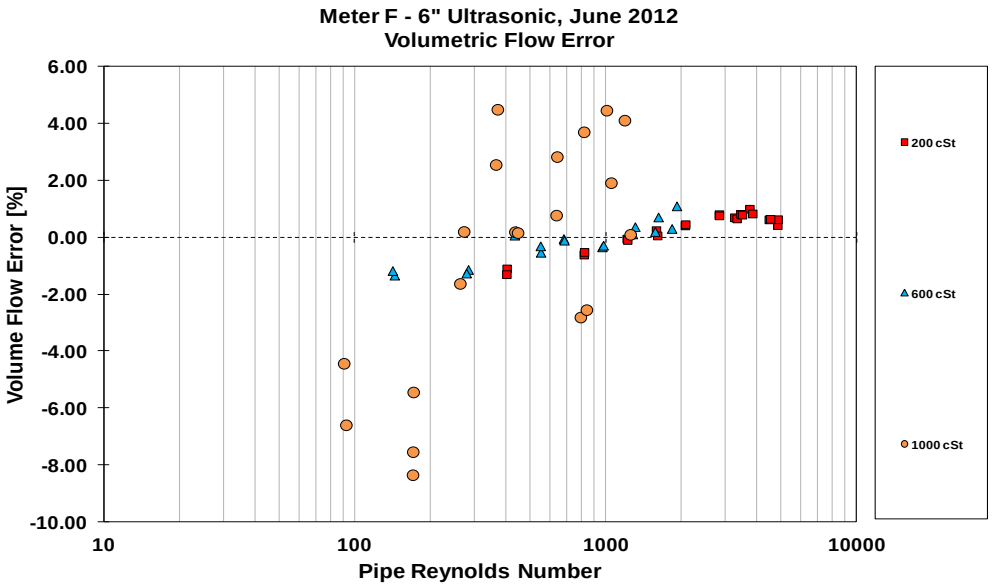

Figure 27 Ultrasonic F – Vol. Flow Error vs. Reynolds number

Meter G

Meter G was equipped with a flow conditioner and 10 diameters of straight pipe immediately upstream. It was originally operated uncorrected.

The volumetric flow errors for Meter G are plotted against reference flowrate in Figure 28. Errors are relatively high, ranging from -2.14 to 2.1 %. There is little correlation of error and viscosity, the highest errors occur for the 200 cSt and 600 cSt (2)[2] series, while the maximum error for the 1000 cSt trend is 0.71 %. There is also no clear trend of errors with flowrate. There is little agreement in errors for the two 600 cSt data series, which suggests that reproducibility is poor for the meter in this case.

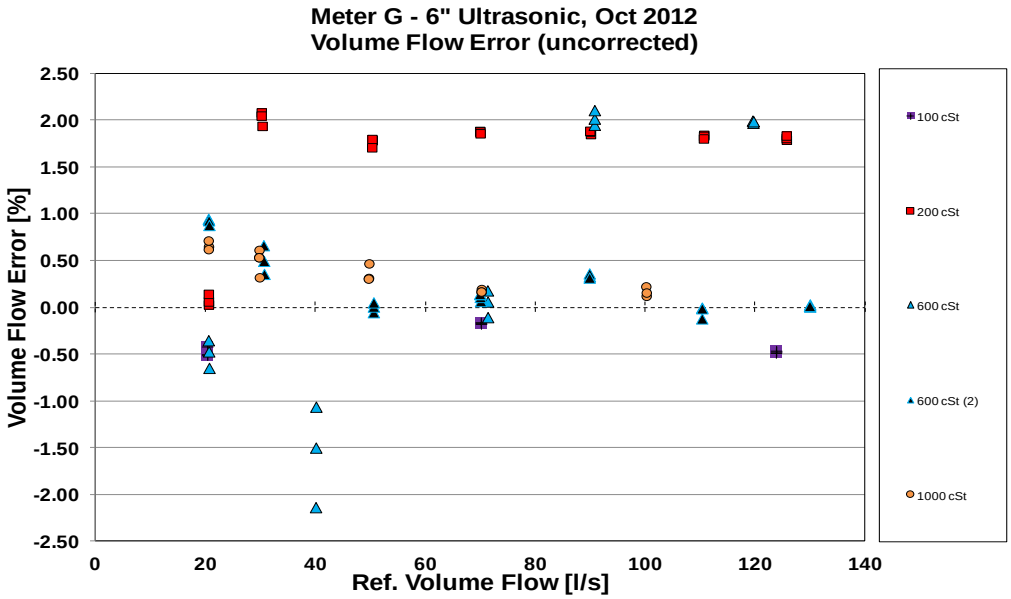

Figure 28 Ultrasonic G – Vol. Flow Error vs. Vol. Flow

[2] (2) corresponds to a repeat of the fluid temperature and viscosity for a different test file.

The uncorrected data for Meter G is plotted against Reynolds number in Figure 29. No clear trends can be observed with regards to viscosity. Individual series seem to display their own trends with Reynolds number. As observed in Figure 28, the two 600 cSt trends show no agreement which suggests poor reproducibility at the test conditions.

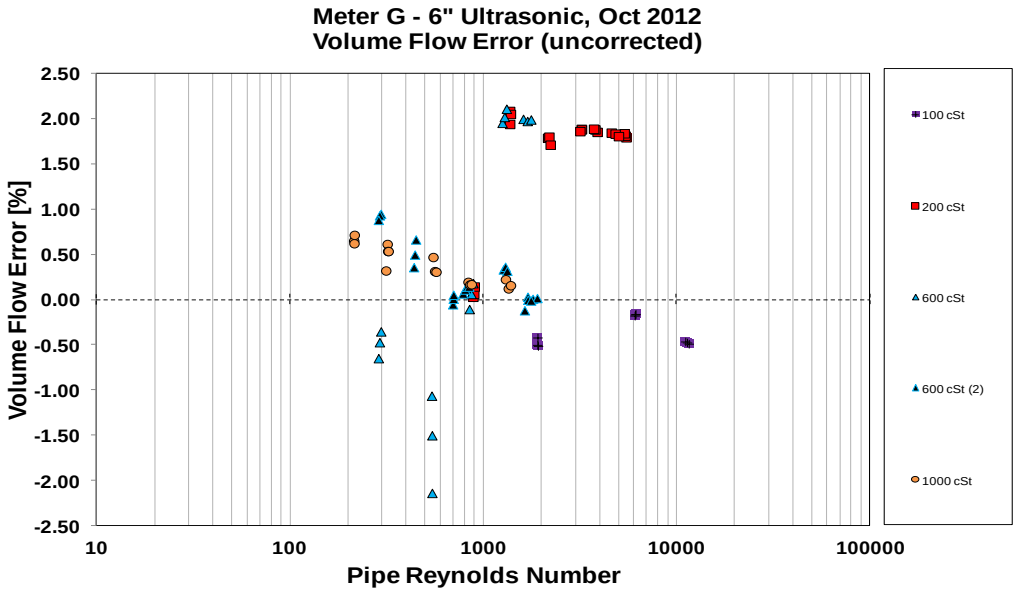

Figure 29 Ultrasonic G – Vol. Flow Error vs. Reynolds number

Corrections were applied to Meter G for Reynolds number effects and the data is shown below in Figure 30. As before, a flow conditioner was installed upstream of the device. Errors are notably lower with the corrections applied. They range from -1 to 1.1 % with most of the data falling within ±0.5 % error. There may be improved reproducibility for the meter with the corrections applied, there are repeat data series for 100 cSt and 200 cSt which show much closer agreement than the two 600 cSt series featured in Figure 28.

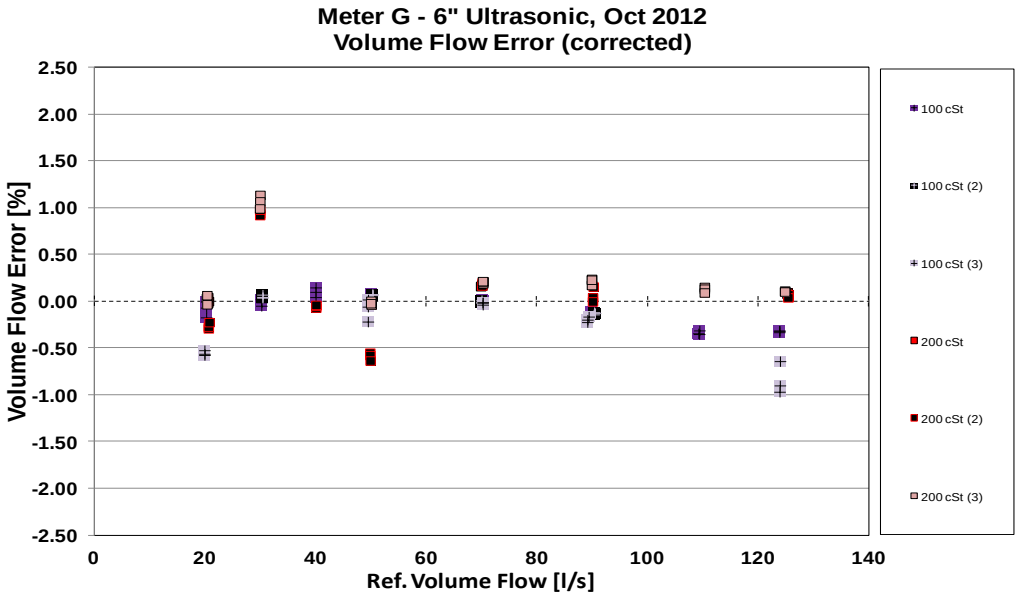

Figure 30 Ultrasonic G – Vol. Flow Error vs. Vol. Flow (corrected)

Figure 31 shows the corrected data with the flow conditioner (FC) plotted against Reynolds number. The maximum errors observed are -0.969 % at Re = 9798 for 100 cSt and 1.136 % at Re = 1174 for 200 cSt. The overall performance is greatly improved over the uncorrected data, the range of errors is lower and the data is less scattered.

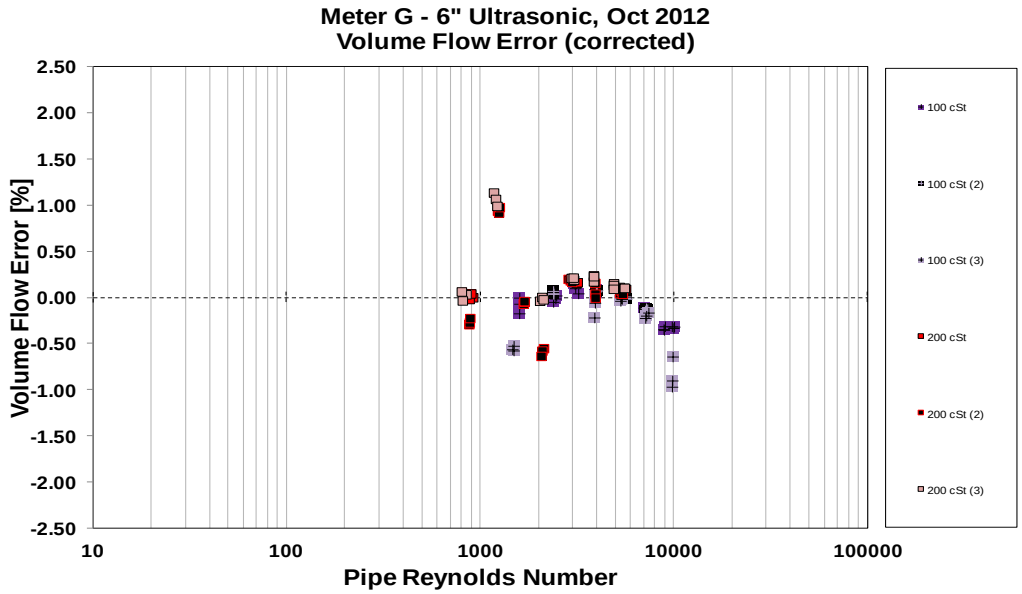

Figure 31 Ultrasonic G – Vol. Flow Error vs. Reynolds number (corrected)

Coriolis Flowmeters

Meter H

Meter H was originally tested with no correction applied. To ensure optimum performance of the device, the meter was zeroed for each temperature and thus viscosity.

The Mass flowrate error data for Meter H is plotted against reference flowrate in Figure 32. Meter H shows errors of approximately -0.4% for most of the flowrates, with a sharp increase to nearly -1% at low flowrates of less than 20 l/s.

There is no clear trend for viscosity differences, but this is limited by the presence of only two sets of data series. The Coriolis under-reading at low Reynolds numbers has been previously reported by NEL [18] and others [7].

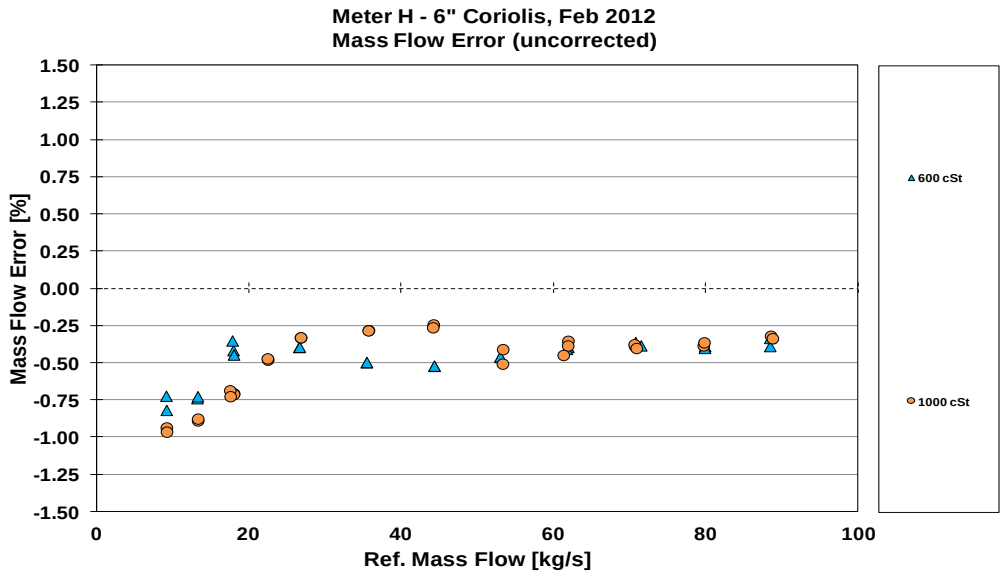

Figure 32 Coriolis H – Mass Flow Error vs. Mass Flow

The uncorrected data for Meter H was plotted against Reynolds number in Figure 33. Most data points have an error between -0.25 and -0.5%, but errors become more negative very sharply as Re decreases below 200. The maximum error of -0.96% occurs at Re of approximately 90. There is close overlap of the two data series despite the large difference in viscosity.

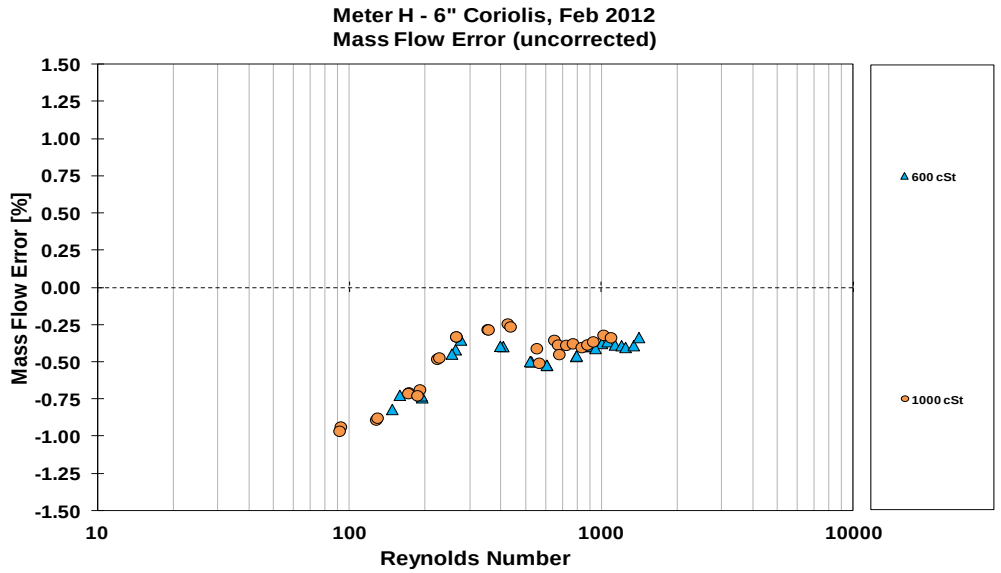

Figure 33 Coriolis H – Mass Flow Error vs. Reynolds number

A Reynolds-based correction was applied to Meter H. As before, the device was zeroed for each temperature and thus viscosity change. The results are shown in Figure 34. The maximum error decreased from -0.96% to -0.55% and for most of the data, errors range from -0.25 to 0.25%.

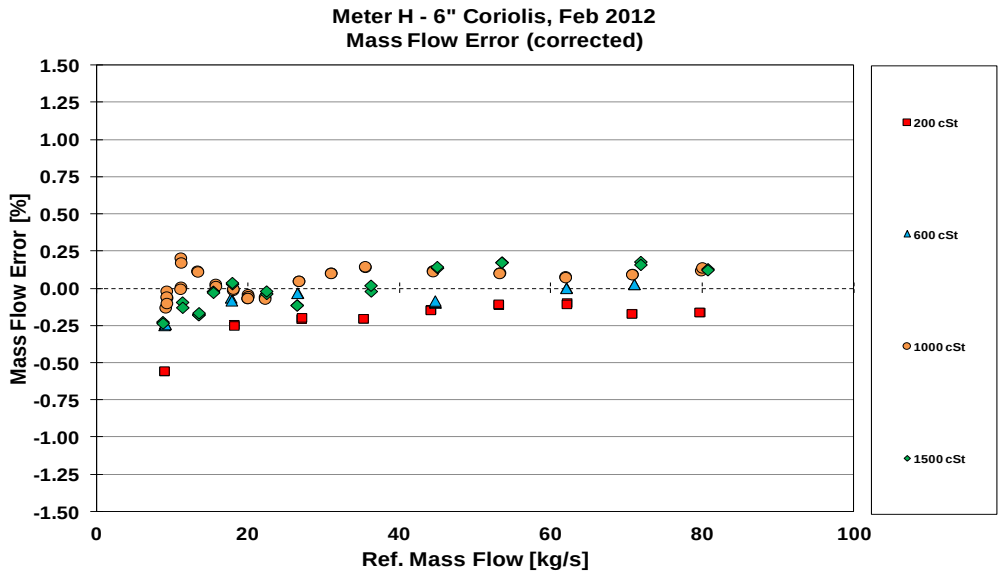

Figure 34 Coriolis H – Mass Flow Error vs. Mass Flow (corrected)

The corrected data for the Meter H mass flow errors has been plotted against Reynolds number in Figure 35. The graph looks largely similar to that plotted against flowrate. Most points have an error between -0.25 and 0.25%, with a maximum error of -0.55% for the 200 cSt condition at Re of approximately 400.

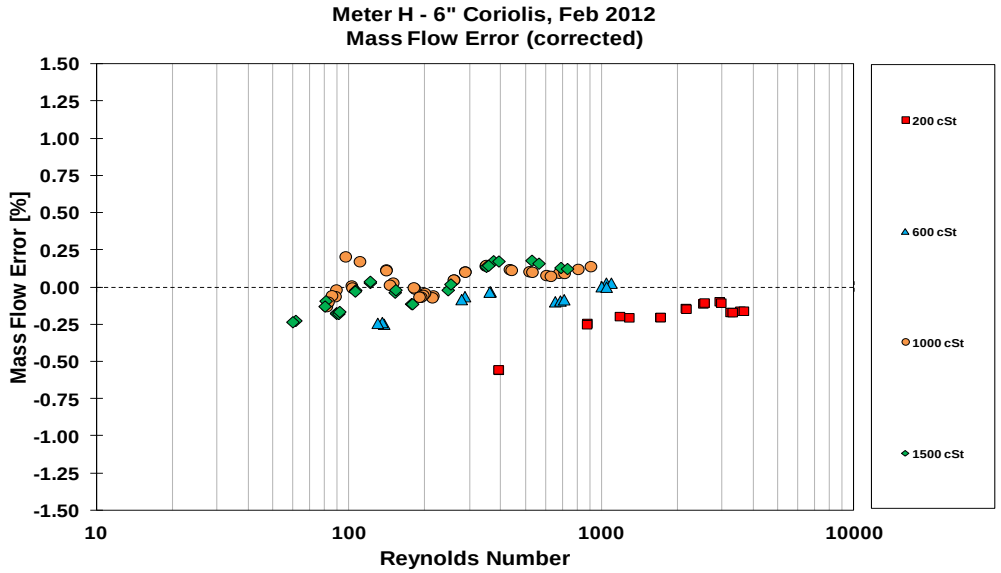

Figure 35 Coriolis H – Mass Flow Error vs. Reynolds number (corrected)

The density errors for Meter H are plotted against reference flowrate in Figure 36. Meter H shows increasingly negative errors in density as flowrate increases. A maximum error of - 0.177 % is observed at approximately 90 kg/s. There is close overlap of the two data series despite the large difference in viscosity.

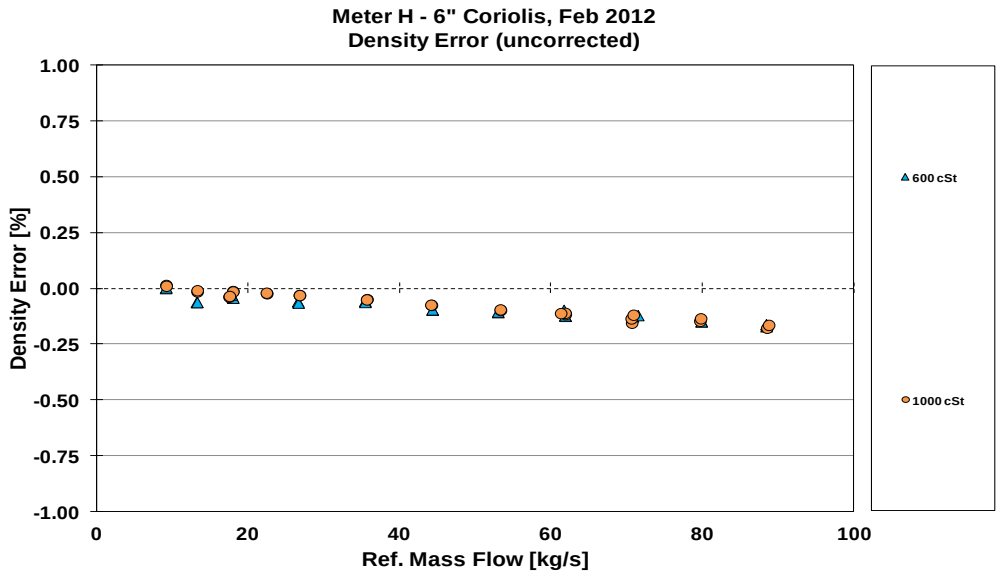

Figure 36 Coriolis H – Density Error vs. Mass Flow

As mentioned previously, a Reynolds based correction was applied to mass flowrate for Meter H. No corrections were applied for density, but additional density data was collected in this period. The "corrected" data for density error is shown in Figure 37. The greatest error in this case was - 0.176 % at 80.7 kg/s. Figure 36 and Figure 37 show that the density measurements of Meter H are repeatable and insensitive to viscosity changes.

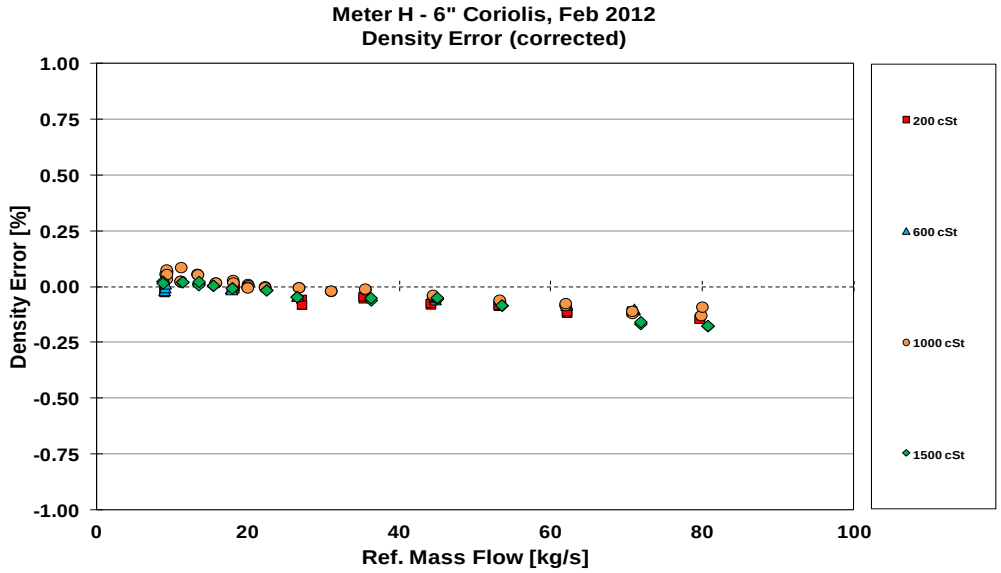

Figure 37 Coriolis H – Density Error vs. Mass Flow (corrected)

Meter I

The mass flow errors for Meter I are plotted against reference flowrate in Figure 38. The greatest error occurs at low flowrates, approximately -0.4% for the 200 cSt test condition, but for most flowrates and viscosities, errors are less than 0.25% in magnitude. It can also be observed that at low flowrates, there is clear separation of data series with different viscosities. This separation is not found as flowrates

increase, and the range of errors decreases from approximately -0.43 and -0.08% to between -0.02 and 0.074%.

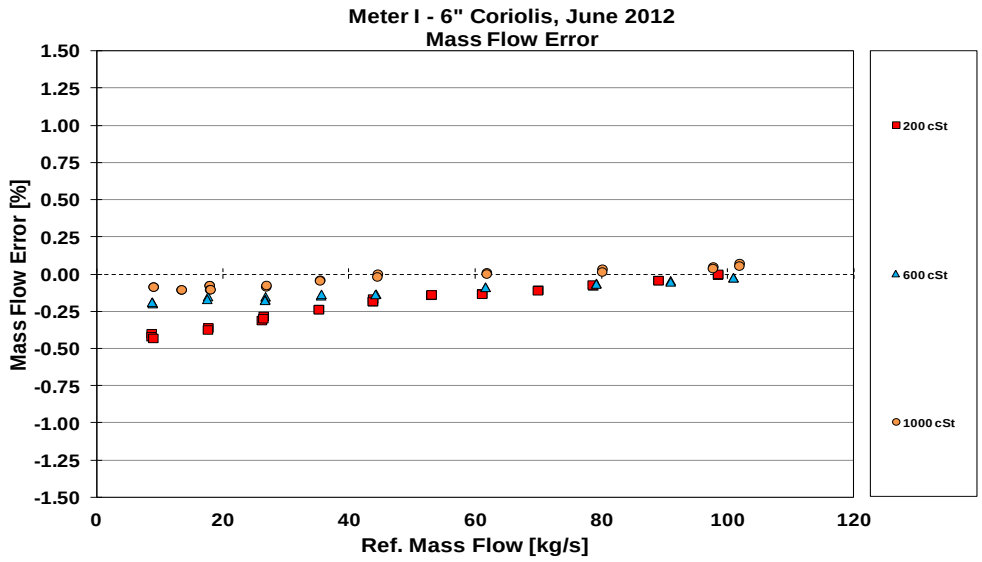

Figure 38 Coriolis I – Mass Flow Error vs. Mass Flow

The mass flow errors for the Meter I were plotted against Reynolds number in Figure 39. The magnitude of the errors decreases as the Reynolds number increases, and a separation of data series based on viscosity differences is observed for the full range of data. Similar to Figure 38, the greatest errors are observed for the 200 cSt data and the smallest errors occur at the 1000 cSt data. The greatest error observed is -0.418% at Re of 430 for the 200 cSt test condition.

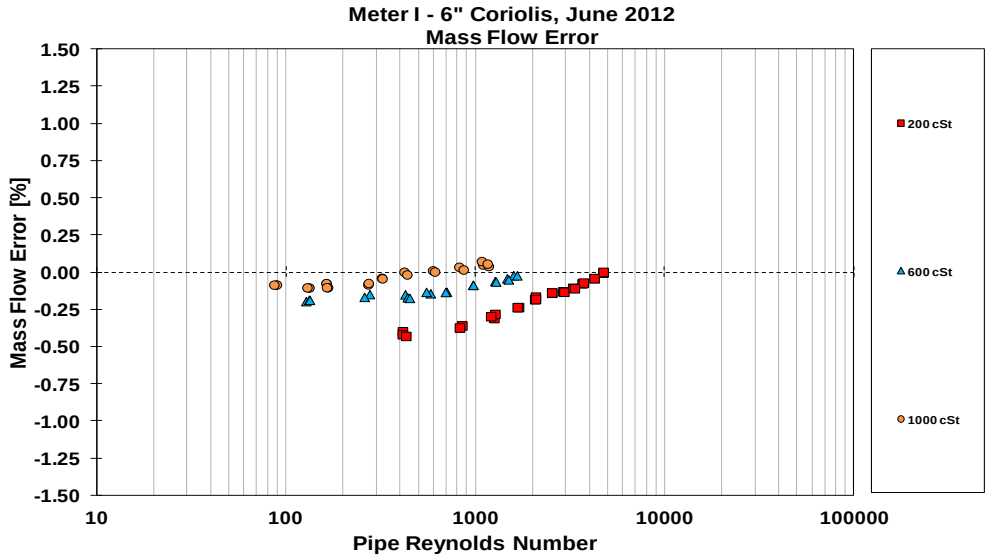

Figure 39 Coriolis I – Mass Flow Error vs. Reynolds number

Density errors for Meter I are plotted against reference flowrate in Figure 40. Density errors for Meter I increase as flowrates increase. The greatest errors are found in the 1000 cSt data series and the smallest errors are found for 200 cSt. The maximum error of 0.454 % is observed at 101 kg/s.

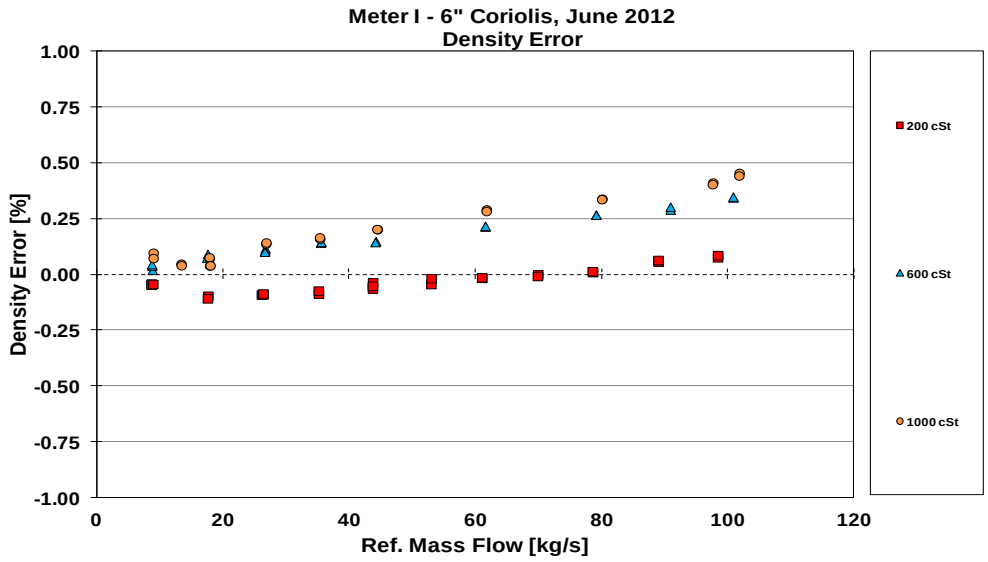

Figure 40 Coriolis I – Density Error vs. Mass Flow

6 SUMMARY AND CONCLUSIONS

A range of commercially available conventional liquid flowmeters have been operated across a range of kinematic viscosities to investigate some of the technical issues likely to be faced as the demand for accurate heavy oil flow measurement grows. When assessing the suitability of a flowmeter for a particularly high viscosity application, the results presented here show that it will be extremely important to calibrate the device in similar conditions as it will encounter in service.

The response of the flowmeters evaluated in this test programme displayed a significant dependence on the liquid viscosity / flow profile. The measurements exhibited distinct trends for each measurement device with increasing fluid viscosity at a given flowrate. The results also clearly demonstrated a relationship with the flow profile. As the Reynolds number of the flow decreased, the response of the device varied significantly.

The discharge coefficients of the **Venturi tubes** were strongly influenced by Reynolds number. The slope of the discharge coefficient tended towards horizontal at high Reynolds numbers. In the transitional and laminar regions, the CD appears to be strongly dependent on Reynolds number. The performance of the Venturi tubes can be characterised by Reynolds number for the full viscosity range. A steady discharge coefficient of 0.995 would typically be expected for turbulent conditions. At Re = 3000 both Venturi tubes showed discharge coefficients of approximately 0.93, representing a flow error of greater than 6.5 % relative to this reference. At Re = 1000, flow error would be greater than 9.5%.

The discharge coefficients of the **Quadrant edge orifice plates** were strongly influenced by the Reynolds number. A near constant discharge coefficient was achieved for Re ≥ 4000 for both sizes. The performance of the orifice plates can be characterised by Reynolds number for the full viscosity range. The “near constant”

experimentally determined discharge coefficients were compared to those calculated from the equation provided in the Shell Flowmeter Engineering Handbook. Discrepancies of 1.58 % and 0.794 % were observed for Meters C and D respectively, which is within the stated 2 % uncertainty of the equation.

Ultrasonic flowmeters generally had high errors when operated uncorrected in the transitional and laminar flow regions. Meter E had a maximum error of approximately 3% with a mean error of approximately 1.5%. Meter F produced spurious readings for the 1000 cSt data set, with errors that were as large as -8%. Meter G had errors ranging from -2.14 to 2.1 %. Corrections applied to Meter E and Meter G improved performance considerably, the maximum error for Meter E decreased to 1.209% and less than 0.5 % error for most of the range of data. Errors for Meter G with corrections applied ranged from -1 to 1.1 % with most of the data falling within ±0.5 %. The behaviour of Meter E changed greatly between the laminar and transition regions.

The **Coriolis** flowmeters had low errors and errors were typically less than 0.75%, even at Reynolds numbers as low as 200. The Coriolis flowmeters seemed unaffected by the laminar-turbulent transition although Meter H showed significant under-read at low Reynolds numbers before the device's correction was applied. The maximum errors were -0.964 and -0.55% for meters H and I respectively. Meter I showed separation of data series of differing viscosities even when plotted against Reynolds number, Meter H did not. With corrections applied, the maximum error observed for Coriolis meters was -0.56%, and the majority of the data was within 0.25% error.

Overall the results reported here reinforce the notion that conventional liquid flowmeters cannot simply be relocated from low viscosity to high viscosity service without suitable consideration, characterisation or modification. The results also show that the performances of devices of the same technology (i.e. ultrasonic) are not necessarily similar as there are many other variables.

7 FUTURE WORK

The test programme in this research project was focussed on testing conventional liquid flowmeters with high viscosity fluids up to 1500 cSt. The next stage of this project could be to research the effects of installation effects (restrictions, upstream bends), temperature gradients within the flow stream under laminar conditions, sensor-signal attenuation. Another area worth exploring is two phase oil & gas flow using a high viscosity fluid. New advancements and the utilisation of multiple technologies might enable accurate determination of the gas volume fraction. It might then be possible to correct for the presence of a second phase within the flow stream.

A future paper by the authors will investigate the pressure drop of various metering technologies when applied to viscous flow. The paper will include calculations for the pressure drop cost for each technology and will also contain an uncertainty analysis for each device to demonstrate the potential financial exposure of each metering technology in viscous flow.

8 REFERENCES

[1] Miller, G. and Belshaw, R. "An investigation into the performance of Coriolis and Ultrasonic Meter at Liquid Viscosities up to 300 cSt", Paper 1.4, 26th International North Sea Flow Measurement Workshop, 21 – 24 October 2008.

[2] Mills, C. and Belshaw, R. "Measurement of Flow in Viscous Fluids using a Helical Blade Turbine", Paper 16, 29th International North Sea Flow Measurement Workshop, 25 – 28 October 2011.

[3] BS EN 5167-1:2003, Measurement of fluid flow by means of pressure differential devices inserted in circular cross-section conduits running full - Part 2: Orifice plates. London, BSI

[4] BS EN 5167-2:2003, Measurement of fluid flow by means of pressure differential devices inserted in circular cross-section conduits running full - Part 2: Orifice plates. London, BSI

[5] Danen, G. and W. A., Shell Flowmeter Engineering Handbook. New York, McGraw Hill, 1985.

[6] Steven, R. "Significantly Improved Capabilities of DP Meter Diagnostics Methodologies", Paper 1.1, 27th International North Sea Flow Measurement Workshop, 20 – 23 October 2008

[7] Tschabold, P. Kumar, V. and Anklin, M. "Influence and Compensation of Process Parameters on Coriolis Meters with a View to Custody Transfer of Hydrocarbon Products". Paper 6.3, 9th South East Asia Hydrocarbon Flow Measurement Workshop, 2 – 4 March 2010.

[8] Coriolis ISO reference BS EN 10790:1999, Measurement of fluid flow in closed conduits -- Guidance to the selection, installation and use of Coriolis meters (mass flow, density and volume flow measurements). London, BSI

[9] Ultrasonic ISO BS EN 12242:2012, Measurement of fluid flow in closed conduits -- Ultrasonic transit-time meters for liquid. London, BSI

[10] BS EN 5167-4:2003, Measurement of fluid flow by means of pressure differential devices inserted in circular cross-section conduits running full - Part 2: Venturi tubes. London, BSI

[11] Mills, C. An Investigation into the effects of high viscosity fluids on conventional liquid flowmeters: Venturi, NEL Report No: 2010/197, 2010.

[12] Stobie, G. Hart, R, Svedeman, S. and Zanker, K. "Erosion in a Venturi Meter with Laminar and Turbulent Flow and Low Reynolds Number Discharge Coefficient Measurements", Paper 15, 25th International North Sea Flow Measurement Workshop, 16 – 19 October 2007.

[13] Benedict, R. P., and J. S. Wyler. A Generalized Discharge Coefficient for Differential Pressure Type Fluid Meters. ASME Journal of Engineering for Power, Vol. 96, 1974.

[14] Shlichting, H. Boundary Layer Theory. New York: McGraw Hill, 1960.

[15] Reynolds, O. On the Dynamical theory of Incompressible Viscous Fluids and the Determination of the Criterion, London: Phil. Trans. Roy. Soc, 1895.

[16] Hall, G.W. Application of Boundary Layer Theory to Explain Some Nozzle and Venturi Flow Peculiarities, Proc.Inst.Mech.Eng, Vol. 173, No.36, 1959.

[17] Linford, A. Flow Measurement & Meters, Taylor & Francis, 1961.

[18] Mills, C. "Measurement of Flow in Viscous Fluids". Oil Sands and Heavy Oil Technologies Conference 2011, 19 – 21 July 2011.